Electronic Supplementary Material (ESI) for Physical Chemistry Chemical Physics.

Electronic Supplementary Information

Detailed mechanism and kinetics of reactions of *anti*- and *syn*-CH_3CHOO with HC(O)OH: Infrared spectra of conformers of hydroperoxyethyl formate

Bedabyas Behera[a] and Yuan-Pern Lee*[ab]

[a]*Department of Applied Chemistry and Institute of Molecular Science, National Yang Ming Chiao Tung University, 1001, Ta-Hsueh Road, Hsinchu 300093, Taiwan.*

[b]*Center for Emergent Functional Matter Science, National Yang Ming Chiao Tung University, Hsinchu 300093, Taiwan*

Emails: bedabyas88@gmail.com (BB); yplee@nycu.edu.tw (YPL)

Table of Contents

A. Section SA Reaction mechanism and error analysis of the rate coefficient k_1 for $CH_3CHOO + HC(O)OH$

The kinetic model, shown in Table S24 (ESI†), considered only the important reactions including the branching of the formation reaction of $CH_3CHI + O_2$, the self-reaction of CH_3CHOO, the reaction of $CH_3CHIOO + CH_3CHOO$, the main reaction of interest $CH_3CHOO + HC(O)OH$ to form HPEF, and the conversion of HPEF to FAA. Other reactions such as reactions of CH_3CHOO with I or IO, wall loss, unimolecular decay of CH_3CHOO, and diffusion loss, which have rate coefficients much less than 1000 s^{-1}, are not included in the model because we are considering a reaction period less than 40 μs. Even for the conversion of HPEF to FAA, reaction 7 in Table S24 (ESI†), with a rate coefficient of ~1420 s^{-1}, it has negligible effect on the rise of HPEF except in a few experiments with very small $[HC(O)OH]_0$, which has an effective pseudo-first-order rate coefficient of ~10^5 s^{-1}. The small error in this rate coefficient, 70 s^{-1} in fitting and perhaps 200 s^{-1} after error analysis, hence has an even smaller effect.

The total rate coefficient of $CH_3CHI + O_2$, 8.6×10^{-12} cm^3 $molecule^{-1}$ s^{-1}, was taken from Howes et al.;[1] a value of 8.0×10^{-12} cm^3 $molecule^{-1}$ s^{-1} was reported by Sheps et al.[2] For the branching involving the formation reaction $CH_3CHI + O_2 \rightarrow CH_3CHOO$ and CH_3CHIOO, reactions 1−3 in Table S24 (ESI†), estimated yields of CH_3CHOO are ~71 and 64 % at 40 and 80 Torr and those of CH_3CHIOO are ~8 and 15 % at 40 and 80 Torr, respectively, according to our unpublished work; about 21 % proceeds to fragmentation and formation of other products. The production of CH_3CHIOO reduces the concentration of CH_3CHOO. When we assumed the concentration of CH_3CHOO to be $[CH_3CHI]_0$, that is, no branching in the formation reaction, the resultant first-order rate coefficient $k_1^{I'}$ decreased by ~7 % and 1 % at the smallest and the largest $[HC(O)OH]_0$ in this work. The effect of the yield of CH_3CHOO is small because

the main reaction CH_3CHOO + HC(O)OH is very rapid, other reactions have limited effect on the main reaction.

Because the presence of CH_3CHIOO, we also included the reaction CH_3CHOO + CH_3CHIOO, reaction 5 in Table S24 (ESI†), even though the rate coefficient has not been reported. When we included this reaction and assumed a rate coefficient of 1×10^{-10} cm^3 $molecule^{-1}$ s^{-1} for this reaction, the fitted first-order rate coefficient $k_1^{I'}$ decreased by ~3 % at the smallest $[HC(O)OH]_0$ and remained nearly the same at larger $[HC(O)OH]_0$.

Rate coefficients for reactions involving I are also unknown. However, because the system has a significant amount of HC(O)OH and its reaction with CH_3CHOO is rapid, I atoms with concentration less than 25 % of HC(O)OH in most cases will not be able to compete with HC(O)OH efficiently. If we include the reactions CH_3CHOO + I using a rate coefficient similar to that of CH_2OO + I (9.0×10^{-12} cm^3 $molecule^{-1}$ s^{-1})[3] and CH_3CHIOO + I using a rate coefficient similar to that of CH_2IOO + I (3.5×10^{-11} cm^3 $molecule^{-1}$ s^{-1})[4] in the model, the fitted first order rate coefficient $k_1^{I'}$ decreased by 3 and 0 % at the smallest and largest $[HC(O)OH]_0$ employed in this work. We hence did not include these reactions in our model.

Considering the errors in the estimation of $[CH_3CHI]_0$ (error <30 % transforms into error <7 % in $k_1^{I'}$), error resulting from uncertainties in the rate coefficient of the self-reaction of CH_3CHOO (k_{self} in Table S24, error 25 % transforms into error ~3 % in $k_1^{I'}$), error due to uncertainties in other reactions (~10 %), and the fitting error (~15 %), the error in $k_1^{I'}$ is estimated to be ~20 %. When we combine the fitting error in Fig. 12 (~20 %) and the error in the absolute concentration of HC(O)OH (20 %), we estimated the overall uncertainty to be ~35 %. A rate coefficient for reaction CH_3CHOO + HC(O)OH at 298 K is hence reported to be k_1 = $(2.1 \pm 0.7)\times10^{-10}$ cm^3 $molecule^{-1}$ s^{-1}.

Table S1 Cartesian coordinates of optimized geometries of six conformers of hydroperoxyethyl formate (HPEF) predicted with the B3LYP/aug-cc-pVTZ method

	x	*y*	*z*		*x*	*y*	*z*
	HPEF (P1)				HPEF (P2)		
O1	0.24707	1.97363	-0.13302	O1	1.95862	-1.21100	-0.36298
O2	-0.61652	1.00822	0.51422	O2	1.67065	0.12561	0.11659
C3	-0.78647	-0.11145	-0.28648	C3	0.34693	0.42677	-0.19009
H4	-0.55502	0.13546	-1.32111	H4	0.10024	0.10774	-1.20016
C5	-2.18156	-0.65098	-0.08336	C5	0.16186	1.91011	0.03037
H6	-2.36381	-0.81959	0.97699	H6	0.42166	2.17466	1.05419
H7	-2.90284	0.07303	-0.45629	H7	0.79766	2.46594	-0.65622
H8	-2.30238	-1.59128	-0.61716	H8	-0.87678	2.17347	-0.15828
O9	0.11325	-1.22057	0.10929	O9	-2.24717	-0.32474	-0.69224
C10	1.43027	-1.06266	0.10104	C10	-1.72310	-0.65875	0.33443
H11	1.91418	-2.01073	0.36135	H11	-2.19859	-1.27965	1.10404
O12	2.04738	-0.05360	-0.14378	O12	-0.48402	-0.33789	0.73338
H13	1.10697	1.50228	-0.10470	H13	1.85697	-1.72673	0.45018
	HPEF (P3)				HPEF (P1*)		
O1	-2.09872	-0.95222	-0.04812	O1	0.96886	1.56536	0.18855
O2	-1.18301	0.02008	-0.61657	O2	0.94308	0.59944	-0.88873
C3	-0.45550	0.59620	0.42492	C3	0.67639	-0.68236	-0.44080
H4	-1.11145	0.76809	1.27570	O4	-1.59959	0.84619	0.50291
C5	0.14834	1.88313	-0.10010	C5	-1.72113	-0.24498	-0.00350
H6	0.69416	1.71392	-1.02285	H6	-2.69383	-0.73445	-0.12794
H7	-0.65260	2.59859	-0.27785	O7	-0.77297	-1.02917	-0.49307
H8	0.82473	2.29390	0.64787	H8	0.00991	1.62788	0.39231
O9	1.80340	-0.52627	-0.89310	H9	1.06059	-1.31610	-1.23822
C10	1.55030	-0.78557	0.24845	C10	1.23741	-1.06383	0.90937
H11	2.14445	-1.46333	0.87643	H11	2.30346	-0.84379	0.92564
O12	0.52143	-0.32831	0.98488	H12	0.75961	-0.51062	1.71241
H13	-1.70294	-1.77992	-0.35556	H13	1.08927	-2.13034	1.06813
	HPEF (P2*)				HPEF (P3*)		
O1	-1.97867	-1.04911	0.30033	O1	2.28764	-0.59264	-0.29344
O2	-1.00413	-0.72550	-0.72649	O2	1.37478	-0.37879	0.81498
C3	-0.28683	0.41928	-0.35503	C3	0.25081	0.31958	0.37387
O4	2.39217	-0.20251	-0.61247	O4	-2.48631	0.12869	0.41687
C5	1.87751	-0.20635	0.46893	C5	-1.85650	-0.58350	-0.31539
H6	2.39417	-0.45514	1.40406	H6	-2.29412	-1.34022	-0.97776
O7	0.59619	0.10194	0.75153	O7	-0.52408	-0.58669	-0.46478
H8	-1.52500	-1.76829	0.76182	H8	2.05193	-1.49564	-0.55036
H9	0.31991	0.60716	-1.23978	H9	-0.30660	0.49345	1.29379
C10	-1.12934	1.60617	0.04574	C10	0.53012	1.60091	-0.37534
H11	-1.83996	1.82894	-0.74854	H11	1.15588	2.24845	0.23725
H12	-1.67411	1.40162	0.96332	H12	1.03992	1.39586	-1.31277
H13	-0.48755	2.47253	0.19801	H13	-0.40985	2.11154	-0.57809

Table S2 Cartesian coordinates of optimized geometries of four conformers of hydroxylated secondary ozonide (HSOZ) predicted with the B3LYP/aug-cc-pVTZ method

	x	*y*	*z*		*x*	*y*	*z*
HSOZ (Q1)				HSOZ (Q2)			
O1	-0.83647	1.20299	-0.15638	O1	-0.78202	1.15715	-0.05975
O2	0.46132	1.06545	0.49615	O2	0.65697	1.19125	0.08789
C3	1.06115	0.11898	-0.36618	C3	0.99946	-0.09636	-0.39764
H4	-1.40999	-0.83969	1.37404	H4	-2.11951	-0.58064	-1.14721
O5	-1.95574	-0.73647	0.58432	O5	-2.27305	-0.55934	-0.19345
C6	-1.20042	-0.15542	-0.40617	C6	-1.12889	-0.14695	0.43242
O7	0.02386	-0.83150	-0.58835	O7	0.00547	-0.94467	0.16896
H8	-1.80975	-0.14232	-1.30856	H8	-1.33355	-0.13075	1.50232
H9	1.31263	0.60282	-1.31625	H9	0.90437	-0.10637	-1.48943
C10	2.25651	-0.50456	0.30306	C10	2.38288	-0.46589	0.06374
H11	2.67114	-1.27245	-0.34795	H11	2.62268	-1.46955	-0.28386
H12	3.02020	0.25166	0.47874	H12	3.11112	0.22914	-0.35260
H13	1.96862	-0.95788	1.24977	H13	2.43522	-0.44174	1.15042
HSOZ (Q1*)				HSOZ (Q2*)			
O1	0.43822	1.02942	0.61098	O1	-0.53061	0.99923	-0.59299
O2	-0.38922	1.08390	-0.59294	O2	0.71725	1.27662	0.08678
C3	-1.00091	-0.19843	-0.54787	C3	1.12894	-0.03551	0.48419
H4	2.04840	-0.03526	-1.12116	H4	-1.15371	0.09235	0.31916
O5	2.22059	-0.27286	-0.20139	O5	-0.08697	-0.70316	0.79991
C6	1.03452	-0.25443	0.49639	C6	1.71153	0.11361	1.39556
O7	0.04782	-1.05963	-0.11133	O7	1.91363	-0.76813	-0.58064
H8	1.25367	-0.58246	1.51080	H8	2.12161	-1.78559	-0.25003
H9	-1.24249	-0.43827	-1.58494	H9	1.34947	-0.80527	-1.51117
C10	-2.21114	-0.26814	0.35620	C10	2.85992	-0.25783	-0.75906
H11	-2.58260	-1.29193	0.39065	H11	-2.10694	-0.62979	-0.33541
H12	-1.95235	0.04923	1.36452	H12	-1.67685	-1.16920	-1.01208
H13	-2.99875	0.37802	-0.03079	H13	-1.64073	0.62881	1.13421

Table S3 Cartesian coordinates of optimized geometries of four pre-reaction complexes of CH_3CHOO and HC(O)OH predicted with the B3LYP/aug-cc-pVTZ method

	x	y	z		x	y	z
		C2				C3	
O1	0.20222	1.77183	-0.18902	O1	-0.10237	1.70945	0.08039
O2	1.11389	0.90437	0.38971	O2	-1.19081	0.94234	-0.30245
C3	1.56384	-0.02459	-0.31905	C3	-1.49579	-0.03374	0.41998
H4	-2.55176	-0.76943	1.22953	H4	2.77685	-0.62183	1.08271
O5	-2.69404	-0.08068	0.56186	O5	2.78213	-0.02048	0.32220
C6	-1.77642	-0.24293	-0.40023	C6	1.71503	-0.30535	-0.43598
O7	-0.96310	-1.13481	-0.41889	O7	0.93635	-1.19910	-0.20582
H8	-1.88659	0.52366	-1.16750	H8	1.67431	0.35832	-1.30024
H9	1.23633	-0.06430	-1.35150	H9	-0.91572	-0.18195	1.32368
C10	2.50000	-0.99892	0.27284	C10	-2.60369	-0.91757	0.01206
H11	2.06850	-1.99984	0.19300	H11	-2.21202	-1.92692	-0.13955
H12	3.43655	-1.00834	-0.29037	H12	-3.34975	-0.97846	0.80792
H13	2.70069	-0.76889	1.31617	H13	-3.06936	-0.56697	-0.90548
		C2*				C4*	
O1	0.98550	1.31637	-0.57236	O1	0.57542	-1.43643	0.38441
O2	1.86642	0.95453	0.42229	O2	1.06613	-0.78657	-0.75135
C3	2.21173	-0.25604	0.48293	C3	1.63524	0.31483	-0.56353
H4	-1.87647	0.02919	-0.00508	H4	-2.08198	0.49334	-0.03827
O5	-1.61744	-1.13354	0.17816	O5	-1.17581	1.26362	-0.27862
C6	2.90288	-0.44754	1.29624	C6	1.96235	0.76986	-1.49276
O7	1.71969	-1.27571	-0.44314	O7	1.86301	0.90539	0.75591
H8	0.64007	-1.40805	-0.29003	H8	0.89414	1.21315	1.15838
H9	1.82629	-0.91106	-1.46826	H9	2.24954	0.13988	1.43171
C10	2.23780	-2.21947	-0.29760	C10	2.52780	1.76174	0.68908
H11	-3.11886	0.53630	0.03934	H11	-1.96616	-0.77888	0.27532
H12	-3.73014	-0.19095	0.23693	H12	-0.99142	-1.05789	0.31115
H13	-1.13152	0.80313	-0.22502	H13	-3.13667	0.79795	-0.06035

Table S4 Cartesian coordinates of optimized geometries of C_2H_5OOH, C_2H_3OOH-1, and C_2H_3OOH-2 predicted with the B3LYP/aug-cc-pVTZ method

	x	*y*	*z*		*x*	*y*	*z*
		C_2H_5OOH				C_2H_3OOH-1	
O1	-1.81571	0.10850	-0.09439	O1	1.70085	0.18984	0.07716
O2	-0.51010	-0.52490	-0.02883	O2	0.46646	-0.50806	-0.23953
C3	0.45998	0.51913	0.02153	C3	-0.57707	0.37051	-0.10431
H4	0.32858	1.17381	-0.84345	H4	1.89321	-0.17183	0.95459
C5	1.81836	-0.15506	0.00440	H5	-0.31073	1.40520	-0.27220
H6	1.94088	-0.81306	0.86440	C6	-1.80336	-0.06986	0.13544
H7	1.94972	-0.74250	-0.90365	H7	-2.62799	0.62568	0.12885
H8	2.60013	0.60409	0.03947	H8	-2.01041	-1.11722	0.30090
H9	0.31771	1.11049	0.93118				
H10	-2.20053	-0.18606	0.74221				
		C_2H_3OOH-2					
O1	-1.30682	-0.57482	-0.09609				
O2	-0.64566	0.70923	-0.01746				
C3	0.71126	0.55494	0.01208				
H4	1.14167	1.54886	0.02959				
C5	1.42355	-0.56118	0.01010				
H6	0.96989	-1.53763	-0.02363				
H7	2.49920	-0.48529	0.03287				
H8	-1.79979	-0.56379	0.73649				

Table S5 Cartesian coordinates of optimized geometries of four conformers of formic acetic anhydride (FAA) and two conformers of formic acid anhydride (FAN) predicted with the B3LYP/aug-cc-pVTZ method

	x	*y*	*z*		*x*	*y*	*z*
		FAA (F1)				FAA (F2)	
C1	2.04832	-0.79923	0.00000	C1	2.04548	-0.48282	0.33450
H2	1.97791	-1.44254	-0.87724	H2	2.30356	-1.28553	-0.35553
H3	1.97792	-1.44253	0.87725	H3	1.88252	-0.93569	1.31349
H4	2.99219	-0.26387	-0.00002	H4	2.85088	0.24244	0.39130
C5	0.91569	0.17939	0.00000	C5	0.78821	0.19644	-0.11263
O6	-0.29703	-0.50314	0.00000	O6	-0.21446	-0.76412	-0.35144
O7	0.99710	1.37289	0.00000	O7	0.62017	1.35689	-0.30542
C8	-1.47363	0.22033	-0.00001	C8	-1.54414	-0.47921	-0.15932
H9	-1.31355	1.30124	-0.00002	H9	-2.13317	-1.21935	-0.71355
O10	-2.52217	-0.33916	0.00000	O10	-1.98585	0.38118	0.53048
		FAA (F3)				FAA (F4)	
C1	0.85764	1.35143	0.24733	C1	1.31459	1.26817	0.00001
H2	0.34428	1.58054	1.17964	H2	0.90771	1.76256	0.88242
H3	0.29814	1.82791	-0.55594	H3	0.90777	1.76254	-0.88244
H4	1.87463	1.73196	0.26692	H4	2.39512	1.36846	0.00004
C5	0.91313	-0.12558	0.00740	C5	0.99308	-0.20305	0.00000
O6	-0.24306	-0.87310	0.35762	O6	-0.34754	-0.59393	0.00001
O7	1.85163	-0.74396	-0.37759	O7	1.80735	-1.07186	-0.00001
C8	-1.51119	-0.44162	0.14337	C8	-1.40307	0.27666	-0.00001
H9	-2.19869	-1.15917	0.60538	H9	-1.12433	1.33572	-0.00005
O10	-1.84306	0.53122	-0.46561	O10	-2.52405	-0.11920	0.00001
		anti-FAN				*syn*-FAN	
O 1	-2.13221	-0.09405	-0.00001	O 1	-1.43419	-0.82189	-0.18971
C 2	-0.97030	-0.33095	0.00001	C 2	-1.20528	0.29117	0.14616
O 3	1.76927	-0.68031	-0.00001	O 3	1.43419	-0.82189	0.18971
C 4	1.29260	0.41201	0.00000	C 4	1.20528	0.29117	-0.14616
H 5	1.85207	1.35344	-0.00001	H 5	1.92265	0.99529	-0.58235
O 6	-0.04730	0.70924	0.00001	O 6	0.00000	0.95820	0.00000
H 7	-0.50396	-1.31881	0.00003	H 7	-1.92264	0.99528	0.58238

Table S6 Harmonic, anharmonic, and scaled harmonic vibrational wavenumbers (cm^{-1}) and IR intensities (km mol^{-1}, listed parenthetically) of conformers P1 and P2 of hydroperoxylethyl formate (HPEF) predicted with the B3LYP/aug-cc-pVTZ method

Mode	P1			P2		
	Harmonic	Anharmonic	Scaled harm.[a]	Harmonic	Anharmonic	Scaled harm[a]
ν_1	3499 (276)	3306	3361 (276)	3739 (41)	3555	3592 (41)
ν_2	3134 (7)	2992	3011 (7)	3133 (5)	3025	3010 (5)
ν_3	3129 (12)	3007	3006 (12)	3130 (11)	2990	3007 (11)
ν_4	3089 (5)	2955	2968 (5)	3102 (2)	2969	2980 (2)
ν_5	3055 (5)	2939	2935 (5)	3054 (5)	2952	2934 (5)
ν_6	3049 (46)	2904	2929 (46)	3029 (53)	2883	2910 (53)
ν_7	1754 (306)	1726	1720 (306)	1784 (310)	1750	1749 (310)
ν_8	1495 (72)	1449	1467 (72)	1491 (4)	1449	1463 (4)
ν_9	1488 (22)	1447	1461 (22)	1488 (5)	1447	1460 (5)
ν_{10}	1485 (8)	1449	1458 (8)	1414 (12)	1389	1388 (12)
ν_{11}	1420 (11)	1383	1394 (11)	1401 (1)	1368	1376 (1)
ν_{12}	1406 (3)	1377	1380 (3)	1383 (7)	1359	1358 (7)
ν_{13}	1364 (8)	1329	1339 (8)	1380 (53)	1334	1355 (53)
ν_{14}	1356 (2)	1321	1331 (2)	1357 (19)	1332	1333 (19)
ν_{15}	1223 (286)	1191	1202 (286)	1208 (78)	1175	1187 (78)
ν_{16}	1176 (41)	1150	1155 (41)	1176 (247)	1145	1156 (247)
ν_{17}	1120 (111)	1089	1102 (111)	1125 (168)	1096	1106 (168)
ν_{18}	1059 (35)	1025	1042 (35)	1063 (51)	1036	1046 (51)
ν_{19}	1050 (1)	1039	1032 (1)	1041 (1)	1017	1024 (1)
ν_{20}	974 (18)	948	959 (18)	961 (15)	936	945 (15)
ν_{21}	871 (26)	855	858 (26)	891 (27)	876	878 (27)
ν_{22}	819 (20)	803	807 (20)	850 (67)	835	838 (67)
ν_{23}	755 (91)	723		748 (16)	732	
ν_{24}	622 (107)	570		549 (16)	541	
ν_{25}	536 (7)	511		504 (3)	498	
ν_{26}	512 (6)	503		399 (4)	394	
ν_{27}	347 (1)	336		330 (35)	442	
ν_{28}	322 (7)	317		255 (96)	95	
ν_{29}	286 (14)	284		242 (21)	235	
ν_{30}	250 (6)	221		212 (1)	315	
ν_{31}	219 (1)	250		202 (2)	84	
ν_{32}	176 (7)	141		139 (4)	139	
ν_{33}	79 (1)	83		49 (3)	49	

[a] Harmonic vibrational wavenumber scaled according to $0.9761\ x + 7.9$, in which x is the harmonic vibrational wavenumber for region 800−2000 cm^{-1}; scaling factor is 0.9607 x for region above 3000 cm^{-1}.

Table S7 Harmonic, anharmonic, and scaled harmonic vibrational wavenumbers (cm^{-1}) and IR intensities (km mol^{-1}, listed parenthetically) of conformer P3 of hydroperoxylethyl formate (HPEF) predicted with the B3LYP/aug-cc-pVTZ method

Mode	P3		
	Harmonic	Anharmonic	Scaled harmonic[a]
ν_1	3749 (42)	3571	3601 (42)
ν_2	3158 (3)	3025	3034 (3)
ν_3	3123 (10)	2989	3000 (10)
ν_4	3094 (14)	2970	2972 (14)
ν_5	3059 (8)	2956	2939 (8)
ν_6	3014 (61)	2874	2896 (61)
ν_7	1795 (291)	1757	1760 (291)
ν_8	1499 (5)	1454	1471 (5)
ν_9	1485 (8)	1439	1457 (8)
ν_{10}	1419 (1)	1381	1393 (1)
ν_{11}	1414 (12)	1374	1388 (12)
ν_{12}	1404 (5)	1346	1379 (5)
ν_{13}	1379 (28)	1408	1354 (28)
ν_{14}	1361 (41)	1295	1336 (41)
ν_{15}	1187 (120)	1157	1167 (120)
ν_{16}	1149 (158)	1113	1130 (158)
ν_{17}	1122 (248)	1094	1103 (248)
ν_{18}	1067 (15)	1035	1049 (15)
ν_{19}	1043 (1)	1016	1026 (1)
ν_{20}	956 (9)	928	941 (9)
ν_{21}	880 (36)	864	867 (36)
ν_{22}	816 (13)	804	804 (13)
ν_{23}	769 (58)	745	
ν_{24}	555 (17)	542	
ν_{25}	516 (9)	510	
ν_{26}	384 (2)	379	
ν_{27}	303 (5)	314	
ν_{28}	234 (11)	236	
ν_{29}	217 (63)	185	
ν_{30}	202 (53)	255	
ν_{31}	193 (4)	122	
ν_{32}	140 (3)	157	
ν_{33}	62 (2)	39	

[a] Harmonic vibrational wavenumber scaled according to $0.9761\,x + 7.9$, in which x is the harmonic vibrational wavenumber; this equation is only valid for wavenumbers below 2000 cm^{-1}. Scaling factor is 0.9607 x for region above 3000 cm^{-1}.

Table S8 Harmonic, anharmonic, and scaled harmonic vibrational wavenumbers (cm^{-1}) and IR intensities (km mol^{-1}, listed parenthetically) of conformers Q1 and Q2 of hydroxylated secondary ozonide (HSOZ) predicted with the B3LYP/aug-cc-pVTZ method

Mode	Q1			Q2		
	Harmonic	Anharmonic	Scaled harmonic[a]	Harmonic	Anharmonic	Scaled harmonic[a]
ν_1	3778 (40)	3602	3629 (40)	3765 (41)	3581	3617 (41)
ν_2	3130 (14)	3004	3007 (14)	3131 (12)	3004	3008 (12)
ν_3	3124 (6)	2988	3001 (6)	3121 (7)	2986	2998 (7)
ν_4	3106 (17)	2967	2984 (17)	3092 (35)	2966	2970 (35)
ν_5	3052 (6)	2945	2932 (6)	3051 (6)	2945	2931 (6)
ν_6	3006 (51)	2894	2888 (51)	2996 (54)	2886	2878 (54)
ν_7	1488 (7)	1452	1460 (7)	1488 (3)	1444	1461 (3)
ν_8	1487 (5)	1448	1459 (5)	1486 (5)	1448	1458 (5)
ν_9	1442 (35)	1406	1416 (35)	1448 (44)	1412	1421 (44)
ν_{10}	1420 (62)	1389	1394 (62)	1425 (84)	1392	1399 (84)
ν_{11}	1397 (15)	1364	1372 (15)	1400 (8)	1365	1374 (8)
ν_{12}	1364 (17)	1335	1339 (17)	1361 (21)	1331	1337 (21)
ν_{13}	1308 (3)	1290	1285 (3)	1322 (28)	1308	1299 (28)
ν_{14}	1288 (15)	1236	1266 (15)	1306 (4)	1248	1283 (4)
ν_{15}	1162 (30)	1133	1142 (30)	1160 (67)	1127	1140 (67)
ν_{16}	1147 (58)	1115	1127 (58)	1159 (212)	1124	1139 (212)
ν_{17}	1121 (106)	1091	1102 (106)	1144 (91)	1111	1125 (91)
ν_{18}	1117 (397)	1080	1099 (397)	1113 (181)	1083	1094 (181)
ν_{19}	994 (54)	965	978 (54)	998 (52)	974	982 (52)
ν_{20}	941 (59)	911	927 (59)	967 (74)	932	952 (74)
ν_{21}	887 (29)	868	874 (29)	943 (9)	918	929 (9)
ν_{22}	875 (2)	858	862 (2)	874 (5)	858	861 (5)
ν_{23}	849 (4)	826	837 (4)	852 (12)	832	839 (12)
ν_{24}	803 (23)	786		743 (30)		
ν_{25}	695 (5)	685		684 (6)		
ν_{26}	560 (18)	548		571 (16)		
ν_{27}	514 (9)	509		491 (1)		
ν_{28}	500 (17)	484		479 (37)		
ν_{29}	316 (1)	301		334 (51)		
ν_{30}	298 (70)	361		279 (11)		
ν_{31}	229 (8)	118		225 (12)		
ν_{32}	197 (2)	241		200 (0)		
ν_{33}	98 (1)	76		78 (1)		

[a] Harmonic vibrational wavenumber scaled according to $0.9761\,x + 7.9$, in which x is the harmonic vibrational wavenumber; this equation is only valid for wavenumbers below 2000 cm^{-1}. Scaling factor is 0.9607 x for region above 3000 cm^{-1}.

Table S9 Harmonic, anharmonic, and scaled harmonic vibrational wavenumbers (cm^{-1}) and IR intensities (km mol^{-1}, listed parenthetically) of conformers P1* and P2* of hydroperoxyethyl formate (HPEF) predicted with the B3LYP/aug-cc-pVTZ method

Mode	P1*			P2*		
	Harmonic	Anharmonic	Scaled harmonic[a]	Harmonic	Anharmonic	Scaled harmonic[a]
ν_1	3473 (293)	3257	3336 (293)	3748 (39)	3571	3601 (39)
ν_2	3149 (7)	3040	3025 (7)	3144 (5)	3028	3021 (5)
ν_3	3127 (8)	3003	3005 (8)	3122 (11)	2999	2999 (11)
ν_4	3095 (6)	2988	2973 (6)	3098 (5)	2973	2976 (5)
ν_5	3060 (6)	2970	2940 (6)	3056 (7)	2960	2936 (7)
ν_6	3045 (49)	2902	2926 (49)	3033 (51)	2889	2914 (51)
ν_7	1748 (285)	1710	1714 (285)	1794 (331)	1760	1759 (331)
ν_8	1494 (85)	1457	1466 (85)	1495 (2)	1450	1467 (2)
ν_9	1490 (15)	1447	1462 (15)	1484 (8)	1436	1457 (8)
ν_{10}	1485 (6)	1438	1457 (6)	1421 (26)	1397	1395 (26)
ν_{11}	1419 (22)	1407	1393 (22)	1401 (3)	1365	1375 (3)
ν_{12}	1411 (2)	1372	1386 (2)	1395 (39)	1382	1369 (39)
ν_{13}	1398 (18)	1357	1372 (18)	1372 (34)	1312	1347 (34)
ν_{14}	1368 (12)	1330	1344 (12)	1349 (2)	1320	1324 (2)
ν_{15}	1212 (231)	1186	1191 (231)	1186 (183)	1153	1165 (183)
ν_{16}	1163 (23)	1127	1143 (23)	1161 (108)	1130	1141 (108)
ν_{17}	1124 (130)	1096	1105 (130)	1105 (172)	1080	1086 (172)
ν_{18}	1058 (25)	1033	1041 (25)	1070 (97)	1042	1052 (97)
ν_{19}	1047 (3)	1032	1030 (3)	1042 (1)	1022	1025 (1)
ν_{20}	940 (14)	918	926 (14)	922 (24)	899	908 (24)
ν_{21}	854 (45)	838	841 (45)	865 (95)	843	852 (95)
ν_{22}	829 (6)	821	817 (6)	838 (16)	826	825 (16)
ν_{23}	712 (110)	734		754 (8)	743	
ν_{24}	662 (84)	664		657 (9)	651	
ν_{25}	616 (26)	483		508 (27)	501	
ν_{26}	469 (16)	468		382 (9)	380	
ν_{27}	421 (5)	420		309 (0)	318	
ν_{28}	315 (1)	325		249 (66)	237	
ν_{29}	266 (12)	264		239 (42)	352	
ν_{30}	255 (5)	254		218 (25)	88	
ν_{31}	231 (2)	304		206 (1)	225	
ν_{32}	193 (5)	140		131 (5)	131	
ν_{33}	74 (1)	117		29 (2)	65	

[a] Harmonic vibrational wavenumber scaled according to $0.9761\,x + 7.9$, in which x is the harmonic vibrational wavenumber; this equation is only valid for wavenumbers below 2000 cm^{-1}. Scaling factor is $0.9607\,x$ for region above 3000 cm^{-1}.

Table S10 Harmonic, anharmonic, and scaled harmonic vibrational wavenumbers (cm^{-1}) and IR intensities (km mol^{-1}, listed parenthetically) of conformer P3* of hydroperoxyethyl formate (HPEF) predicted with the B3LYP/aug-cc-pVTZ method

Mode	P3*		
	Harmonic	Anharmonic	Scaled harmonic[a]
ν_1	3742 (41)	3558	3595 (41)
ν_2	3144 (5)	3022	3021 (5)
ν_3	3122 (10)	2995	2999 (10)
ν_4	3092 (4)	2971	2971 (4)
ν_5	3056 (6)	2958	2936 (6)
ν_6	3035 (50)	2888	2916 (50)
ν_7	1783 (322)	1749	1749 (322)
ν_8	1493 (1)	1450	1465 (1)
ν_9	1488 (8)	1433	1460 (8)
ν_{10}	1416 (29)	1390	1390 (29)
ν_{11}	1400 (2)	1369	1374 (2)
ν_{12}	1383 (66)	1375	1358 (66)
ν_{13}	1376 (11)	1335	1351 (11)
ν_{14}	1349 (2)	1306	1325 (2)
ν_{15}	1198 (264)	1166	1177 (264)
ν_{16}	1160 (30)	1133	1140 (30)
ν_{17}	1125 (166)	1093	1106 (166)
ν_{18}	1069 (79)	1042	1051 (79)
ν_{19}	1040 (0)	1019	1023 (0)
ν_{20}	923 (28)	898	909 (28)
ν_{21}	874 (95)	851	861 (95)
ν_{22}	852 (13)	838	840 (13)
ν_{23}	744 (8)	729	
ν_{24}	633 (7)	626	
ν_{25}	502 (23)	500	
ν_{26}	412 (16)	406	
ν_{27}	298 (8)	274	
ν_{28}	266 (94)	419	
ν_{29}	250 (31)	67	
ν_{30}	231 (3)	322	
ν_{31}	201 (3)	102	
ν_{32}	123 (6)	137	
ν_{33}	32 (3)	32	

[a] Harmonic vibrational wavenumber scaled according to $0.9761\,x + 7.9$, in which x is the harmonic vibrational wavenumber; this equation is only valid for wavenumbers below 2000 cm^{-1}. Scaling factor is $0.9607\,x$ for region above 3000 cm^{-1}.

Table S11 Harmonic, anharmonic, and scaled harmonic vibrational wavenumbers (cm^{-1}) and IR intensities (km mol^{-1}, listed parenthetically) of conformers Q1* and Q2* of hydroxylated secondary ozonide (HSOZ) predicted with the B3LYP/aug-cc-pVTZ method

Mode	Q1*			Q2*		
	Harmonic	Anharmonic	Scaled harmonic[a]	Harmonic	Anharmonic	Scaled harmonic[a]
ν_1	3779 (45)	3601	3630 (45)	3765 (40)	3587	3617 (40)
ν_2	3128 (12)	2999	3005 (12)	3123 (17)	2993	3000 (17)
ν_3	3113 (8)	2962	2991 (8)	3111 (11)	2975	2989 (11)
ν_4	3112 (15)	2989	2990 (15)	3079 (42)	2953	2958 (42)
ν_5	3061 (16)	2931	2941 (16)	3053 (22)	2924	2933 (22)
ν_6	3045 (7)	2946	2926 (7)	3043 (7)	2942	2923 (7)
ν_7	1489 (3)	1446	1462 (3)	1489 (4)	1443	1461 (4)
ν_8	1486 (5)	1440	1458 (5)	1486 (8)	1446	1458 (8)
ν_9	1434 (49)	1395	1408 (49)	1442 (83)	1405	1416 (83)
ν_{10}	1413 (50)	1387	1388 (50)	1412 (47)	1385	1387 (47)
ν_{11}	1385 (17)	1352	1360 (17)	1389 (17)	1358	1364 (17)
ν_{12}	1336 (20)	1299	1312 (20)	1349 (22)	1318	1324 (22)
ν_{13}	1302 (7)	1277	1278 (7)	1325 (12)	1292	1301 (12)
ν_{14}	1275 (15)	1234	1252 (15)	1303 (7)	1261	1280 (7)
ν_{15}	1150 (28)	1123	1130 (28)	1173 (245)	1136	1153 (245)
ν_{16}	1117 (10)	1082	1098 (10)	1147 (34)	1121	1127 (34)
ν_{17}	1114 (572)	1077	1095 (572)	1116 (222)	1079	1098 (222)
ν_{18}	1076 (41)	1049	1058 (41)	1088 (67)	1060	1070 (67)
ν_{19}	992 (40)	965	976 (40)	1002 (41)	977	986 (41)
ν_{20}	943 (79)	912	928 (79)	963 (65)	930	948 (65)
ν_{21}	885 (9)	861	871 (9)	930 (4)	908	916 (4)
ν_{22}	872 (13)	852	859 (13)	892 (26)	869	879 (26)
ν_{23}	848 (5)	830	836 (5)	844 (3)	826	832 (3)
ν_{24}	800 (21)	784		748 (11)	737	
ν_{25}	745 (1)	733		705 (11)	694	
ν_{26}	564 (15)	556		560 (12)	552	
ν_{27}	544 (21)	532		483 (14)	483	
ν_{28}	468 (14)	460		463 (30)	449	
ν_{29}	349 (6)	390		379 (8)	379	
ν_{30}	290 (64)	258		311 (64)	306	
ν_{31}	230 (0)	210		235 (0)	285	
ν_{32}	196 (8)	149		209 (3)	133	
ν_{33}	95 (1)	97		78 (1)	78	

[a] Harmonic vibrational wavenumber scaled according to $0.9761\ x + 7.9$, in which x is the harmonic vibrational wavenumber; this equation is only valid for wavenumbers below 2000 cm^{-1}. Scaling factor is 0.9607 x for region above 3000 cm^{-1}.

Table S12 Harmonic, anharmonic, and scaled harmonic vibrational wavenumbers (cm^{-1}) and IR intensities (km mol^{-1}, listed parenthetically) of C_2H_5OOH predicted with the B3LYP/aug-cc-pVTZ method

Mode	C_2H_5OOH		
	Harmonic	Anharmonic	Scaled harmonic[a]
ν_1	3755 (38)	3571	3607 (38)
ν_2	3110 (28)	2971	2988 (28)
ν_3	3104 (21)	2989	2982 (21)
ν_4	3044 (28)	2900	2925 (28)
ν_5	3040 (15)	2907	2920 (15)
ν_6	3005 (42)	2857	2887 (42)
ν_7	1528 (6)	1490	1499 (6)
ν_8	1501 (4)	1457	1473 (4)
ν_9	1483 (6)	1440	1456 (6)
ν_{10}	1414 (5)	1390	1388 (5)
ν_{11}	1391 (0)	1370	1366 (0)
ν_{12}	1360 (57)	1310	1336 (57)
ν_{13}	1276 (1)	1243	1253 (1)
ν_{14}	1183 (5)	1162	1163 (5)
ν_{15}	1150 (23)	1121	1131 (23)
ν_{16}	1035 (17)	1003	1019 (17)
ν_{17}	951 (6)	927	936 (6)
ν_{18}	868 (8)	853	855 (8)
ν_{19}	829 (1)	823	817 (1)
ν_{20}	474 (8)	468	
ν_{21}	296 (0)	293	
ν_{22}	232 (5)	217	
ν_{23}	188 (103)	100	
ν_{24}	127 (6)	121	

[a] Harmonic vibrational wavenumber scaled according to $0.9761\ x + 7.9$, in which x is the harmonic vibrational wavenumber; this equation is only valid for wavenumbers below 2000 cm^{-1}. Scaling factor is $0.9607\ x$ for region above 3000 cm^{-1}.

Table S13 Harmonic, anharmonic, and scaled harmonic vibrational wavenumbers (cm^{-1}) and IR intensities (km mol^{-1}, listed parenthetically) of C_2H_3OOH-1 and C_2H_3OOH-2 predicted with the B3LYP/aug-cc-pVTZ method

Mode	C_2H_3OOH-1			C_2H_3OOH-2		
	Harmonic	Anharmonic	Scaled harmonic[a]	Harmonic	Anharmonic	Scaled harmonic[a]
ν_1	3736 (39)	3553	3589 (39)	3752 (56)	3572	3604 (56)
ν_2	3253 (2)	3115	3125 (2)	3270 (1)	3131	3142 (1)
ν_3	3189 (3)	3054	3063 (3)	3186 (1)	3048	3061 (1)
ν_4	3161 (1)	3064	3037 (1)	3171 (0)	2998	3047 (0)
ν_5	1683 (90)	1641	1651 (90)	1697 (138)	1650	1664 (138)
ν_6	1423 (3)	1391	1396 (3)	1431 (19)	1423	1404 (19)
ν_7	1370 (47)	1339	1345 (47)	1379 (36)	1321	1354 (36)
ν_8	1317 (2)	1293	1294 (2)	1324 (3)	1292	1301 (3)
ν_9	1181 (67)	1153	1161 (67)	1151 (40)	1128	1132 (40)
ν_{10}	993 (29)	981	977 (29)	971 (18)	917	956 (18)
ν_{11}	970 (10)	935	954 (10)	969 (24)	972	954 (24)
ν_{12}	884 (51)	870	870 (51)	892 (31)	867	879 (31)
ν_{13}	872 (25)	843	859 (25)	865 (59)	846	852 (59)
ν_{14}	711 (9)	689		709 (6)	695	
ν_{15}	527 (8)	521		621 (5)	611	
ν_{16}	347 (2)	343		320 (0)	315	
ν_{17}	237 (106)	146		243 (5)	229	
ν_{18}	92 (17)	64		131 (122)	119	

[a] Harmonic vibrational wavenumber scaled according to $0.9761\,x + 7.9$, in which x is the harmonic vibrational wavenumber; this equation is only valid for wavenumbers below 2000 cm^{-1}. Scaling factor is 0.9607 x for region above 3000 cm^{-1}.

Table S14 Rotational parameters of the ground state and vibrationally excited states (v = 1) and ratios of *a*-, *b*-, and *c*-types of conformers P1 and P2 of HPEF predicted with the B3LYP/aug-cc-pVTZ method

Mode	HPEF (P1)				HPEF (P2)			
	A'/*A*"	*B*'/*B*"	*C*'/*C*"	*a*-/*b*-/*c*-	*A*'/*A*"	*B*'/*B*"	*C*'/*C*"	*a*-/*b*-/*c*-
ν_1	1.011	0.997	1.000	66/34/0	1.001	1.000	1.000	5/57/38
ν_7	1.000	0.999	0.999	61/37/1	1.001	0.998	0.999	55/0/44
ν_8	0.996	1.002	1.000	9/80/11	1.001	1.000	1.001	25/2/73
ν_9	0.999	1.000	1.001	1/98/1	1.000	1.001	1.001	0/4/96
ν_{10}	1.000	1.001	1.000	1/21/78	0.999	0.999	0.999	1/99/1
ν_{11}	1.000	0.998	0.999	92/6/2	1.000	1.000	1.001	21/1/78
ν_{12}	0.999	1.001	1.000	36/60/4	1.002	0.998	1.003	52/21/26
ν_{13}	0.999	1.000	0.999	81/17/2	0.999	0.999	1.000	21/76/3
ν_{14}	0.999	1.000	0.999	41/16/42	1.002	0.996	0.993	28/72/1
ν_{15}	0.999	0.998	0.998	98/0/2	0.997	0.999	0.999	71/29/0
ν_{16}	1.002	1.000	0.999	70/17/13	1.001	0.999	0.999	86/12/2
ν_{17}	0.996	0.999	0.999	34/62/5	0.996	0.999	0.999	100/0/0
ν_{18}	0.999	0.998	0.998	79/5/16	0.997	0.999	0.998	38/39/23
ν_{19}	1.000	0.999	1.000	5/23/72	1.000	1.000	0.999	43/39/18
ν_{20}	0.998	0.999	0.999	67/31/2	0.997	1.000	0.999	47/50/4
ν_{21}	0.998	1.000	0.999	24/73/3	0.999	0.999	0.998	100/0/0
ν_{22}	1.001	0.998	0.999	17/79/5	0.997	0.999	0.999	65/13/22
v = 0	A" / cm^{-1}	B" / cm^{-1}	C" / cm^{-1}		A" / cm^{-1}	B" / cm^{-1}	C" / cm^{-1}	
	0.1188	0.0845	0.0524		0.1344	0.0638	0.0496	

Table S15 Rotational parameters of the ground state and vibrationally excited states (v = 1) and ratios of *a*-, *b*-, and *c*-types of the conformer P3 of HPEF predicted with the B3LYP/aug-cc-pVTZ method

Mode	HPEF (P3)			
	A'/*A*"	*B*'/*B*"	*C*'/*C*"	*a*-/*b*-/*c*-
ν_1	1.001	0.999	0.999	0/93/7
ν_7	0.998	1.000	1.000	27/0/73
ν_8	1.002	0.999	1.000	17/32/51
ν_9	1.001	1.000	1.000	13/0/86
ν_{10}	1.002	0.999	1.001	8/1/92
ν_{11}	0.997	1.000	1.000	1/83/16
ν_{12}	1.001	1.000	1.001	39/2/59
ν_{13}	1.000	0.998	0.998	42/56/2
ν_{14}	0.996	1.000	0.999	50/49/1
ν_{15}	1.001	1.000	0.999	44/27/29
ν_{16}	0.999	0.999	0.999	54/42/3
ν_{17}	0.999	0.997	0.999	91/8/1
ν_{18}	0.995	1.000	0.999	36/64/0
ν_{19}	1.000	1.000	0.999	88/10/2
ν_{20}	1.000	0.998	0.998	24/69/7
ν_{21}	1.000	0.998	0.998	76/2/21
ν_{22}	1.002	0.996	0.997	81/0/19
	A" / cm^{-1}	*B*" / cm^{-1}	*C*" / cm^{-1}	
v = 0	0.1211	0.0722	0.0583	

Table S16 Rotational parameters of the ground state and vibrationally excited states (v = 1) and ratios of *a*-, *b*-, and *c*-types of conformers Q1 and Q2 of HSOZ predicted with the B3LYP/aug-cc-pVTZ method

Mode	HSOZ (Q1)				HSOZ (Q2)			
	A'/*A*"	*B*'/*B*"	*C*'/*C*"	*a*-/*b*-/*c*-	*A*'/*A*"	*B*'/*B*"	*C*'/*C*"	*a*-/*b*-/*c*-
ν_1	1.001	0.999	0.999	4/8/88	1.000	1.000	1.000	10/2/88
ν_7	1.001	1.001	1.000	0/1/99	1.000	1.000	1.001	35/62/3
ν_8	1.000	1.000	1.001	23/60/17	1.000	1.001	1.000	0/1/99
ν_9	0.999	1.001	1.002	32/32/36	1.000	1.000	1.001	85/12/3
ν_{10}	0.999	1.000	1.001	100/0/0	1.000	0.999	1.001	99/1/1
ν_{11}	0.999	1.000	1.002	95/3/2	1.000	0.999	1.001	93/2/5
ν_{12}	0.999	0.999	0.996	28/65/7	0.999	1.000	0.997	0/99/1
ν_{13}	0.999	1.000	1.000	73/9/18	1.000	1.000	0.999	87/8/5
ν_{14}	0.999	1.000	0.999	55/44/1	0.998	1.000	1.000	11/67/23
ν_{15}	1.000	1.001	1.000	21/3/75	0.999	1.000	0.999	94/3/3
ν_{16}	0.996	1.000	1.003	1/98/1	0.999	1.000	1.000	77/11/12
ν_{17}	0.996	0.999	1.000	57/1/42	1.001	0.999	1.001	49/50/0
ν_{18}	0.997	0.998	0.999	76/14/10	0.996	0.997	0.997	84/7/9
ν_{19}	1.000	0.998	1.001	48/12/40	1.003	0.998	1.000	43/2/55
ν_{20}	0.998	0.999	0.998	3/85/12	0.995	0.999	0.997	6/93/1
ν_{21}	0.999	0.999	1.000	8/89/4	0.997	0.999	0.999	16/26/58
ν_{22}	0.999	1.000	1.000	3/7/90	1.000	1.000	0.998	0/99/0
ν_{23}	0.998	0.998	0.997	0/1/99	0.998	0.999	0.999	42/56/2
ν_{24}	1.002	0.998	0.997	23/60/17	1.000	0.999	1.000	55/23/22
	A" / cm^{-1}	*B*" / cm^{-1}	*C*" / cm^{-1}		*A*" / cm^{-1}	*B*" / cm^{-1}	*C*" / cm^{-1}	
v = 0	0.1747	0.0754	0.0636		0.2037	0.0706	0.0571	

Table S17 Rotational parameters of the ground state and vibrationally excited states (v = 1) and ratios of *a*-, *b*-, and *c*-types of conformers P1* and P2* of HPEF predicted with the B3LYP/aug-cc-pVTZ method

Mode	HPEF (P1*)				HPEF (P2*)			
	A'/*A*"	*B*'/*B*"	*C*'/*C*"	*a*-/*b*-/*c*-	*A*'/*A*"	*B*'/*B*"	*C*'/*C*"	*a*-/*b*-/*c*-
ν_1	1.001	1.004	0.998	96/1/3	1.004	0.997	0.998	1/73/26
ν_7	0.999	1.000	1.000	7/78/14	1.002	0.996	0.998	58/2/40
ν_8	1.000	0.999	0.999	13/63/24	1.000	1.000	1.001	25/30/45
ν_9	1.001	1.001	1.000	13/76/10	1.002	1.000	1.000	10/4/86
ν_{10}	1.001	1.001	1.000	43/19/38	0.998	0.999	0.999	1/97/2
ν_{11}	0.998	0.999	1.000	21/13/66	1.000	1.000	1.001	41/0/59
ν_{12}	1.001	0.999	1.000	9/82/10	1.003	0.998	1.000	52/36/12
ν_{13}	1.000	1.001	1.002	39/55/7	0.998	1.002	1.001	44/5/52
ν_{14}	0.998	0.997	0.997	41/32/28	0.996	0.999	0.997	28/53/18
ν_{15}	0.999	0.998	0.999	77/22/1	0.997	1.002	1.000	83/16/1
ν_{16}	1.002	1.000	1.000	32/1/67	0.997	1.000	1.000	92/7/1
ν_{17}	0.995	0.999	1.000	85/5/10	0.996	1.001	1.001	93/4/3
ν_{18}	0.999	0.998	0.999	85/10/5	0.998	0.998	0.998	69/21/10
ν_{19}	0.999	1.000	0.999	94/3/2	0.999	1.000	0.999	55/45/0
ν_{20}	0.999	0.999	0.999	1/0/0	0.999	0.999	0.999	66/8/27
ν_{21}	0.997	1.000	0.999	66/34/0	0.996	1.000	0.999	81/5/13
ν_{22}	0.999	0.999	1.000	70/3/27	0.996	1.002	1.000	14/10/76
	A" / cm^{-1}	*B*" / cm^{-1}	*C*" / cm^{-1}		*A*" / cm^{-1}	*B*" / cm^{-1}	*C*" / cm^{-1}	
v = 0	0.1167	0.0856	0.0643		0.1499	0.0598	0.0518	

Table S18 Rotational parameters of the ground state and vibrationally excited states (v = 1) and ratios of *a*-, *b*-, and *c*-types of the conformer P3* of HPEF predicted with the B3LYP/aug-cc-pVTZ method

Mode	HPEF (P3*)			
	A'/*A*"	*B*'/*B*"	*C*'/*C*"	*a*-/*b*-/*c*-
ν_1	1.000	1.001	1.000	3/85/12
ν_7	1.002	0.999	0.999	70/11/19
ν_8	1.000	1.000	1.000	85/8/7
ν_9	1.000	1.000	1.000	11/14/76
ν_{10}	0.999	1.000	0.999	0/84/15
ν_{11}	1.000	1.001	1.000	40/12/48
ν_{12}	1.000	0.999	1.000	57/18/24
ν_{13}	1.009	0.999	1.001	18/12/70
ν_{14}	0.994	1.000	0.997	75/17/8
ν_{15}	0.997	0.997	0.998	91/9/0
ν_{16}	1.002	1.001	1.000	80/1/19
ν_{17}	0.991	0.997	0.999	93/2/5
ν_{18}	0.997	0.999	0.999	60/37/4
ν_{19}	0.999	1.000	1.000	49/47/4
ν_{20}	0.998	1.000	0.999	56/25/19
ν_{21}	0.997	0.997	0.998	88/2/10
ν_{22}	0.996	0.999	0.999	1/70/30
	A" / cm^{-1}	B" / cm^{-1}	C" / cm^{-1}	
v = 0	0.1754	0.0551	0.0491	

Table S19 Rotational parameters of the ground state and vibrationally excited states (v = 1) and ratios of *a*-, *b*-, and *c*-types of conformers Q1* and Q2* of HSOZ predicted with the B3LYP/aug-cc-pVTZ method

Mode	HSOZ (Q1*)				HSOZ (Q2*)			
	A'/*A*"	*B*'/*B*"	*C*'/*C*"	*a*-/*b*-/*c*-	*A*'/*A*"	*B*'/*B*"	*C*'/*C*"	*a*-/*b*-/*c*-
ν_1	1.000	1.000	1.000	7/4//89	0.999	1.000	1.003	0/48/52
ν_7	1.001	1.000	1.001	11/82/7	1.003	0.999	1.000	1/13/87
ν_8	1.000	1.001	1.000	12/1/88	1.000	1.001	1.000	47/18/36
ν_9	1.000	1.000	1.001	96/3/1	1.000	1.000	1.001	73/15/12
ν_{10}	0.999	0.999	1.000	85/1/14	0.998	0.999	1.000	69/14/17
ν_{11}	0.999	1.000	1.003	97/3/0	0.999	1.000	1.003	96/4/0
ν_{12}	1.000	1.000	0.997	7/92/1	0.997	1.000	0.999	5/88/8
ν_{13}	1.000	1.000	1.000	93/4/3	0.998	1.000	1.000	88/2/10
ν_{14}	0.999	1.000	0.997	99/0/1	0.997	1.000	0.999	72/6/22
ν_{15}	1.003	1.002	0.999	30/1/69	0.995	1.001	1.001	72/17/11
ν_{16}	0.999	0.996	1.000	19/17/63	1.003	1.002	0.999	63/1/36
ν_{17}	0.999	0.998	1.000	98/0/2	0.997	0.997	1.004	97/1/1
ν_{18}	0.997	1.000	0.998	6/94/0	0.993	1.001	0.999	5/75/20
ν_{19}	1.002	0.998	1.000	3/6/91	0.999	1.000	1.001	45/3/52
ν_{20}	0.995	0.999	0.998	1/95/4	0.999	0.997	0.997	17/73/10
ν_{21}	0.999	1.000	0.999	31/63/6	0.999	1.000	1.001	2/35/63
ν_{22}	0.998	0.999	0.999	4/96/0	0.995	1.000	1.000	1/99/0
ν_{23}	0.998	0.999	0.999	11/82/7	1.000	0.998	0.997	57/9/34
ν_{24}	1.000	0.999	1.000	12/1/88	1.003	0.998	0.998	14/49/38
	A" / cm^{-1}	*B*" / cm^{-1}	*C*" / cm^{-1}		*A*" / cm^{-1}	*B*" / cm^{-1}	*C*" / cm^{-1}	
v = 0	0.1900	0.0748	0.0657		0.1635	0.0779	0.0665	

Table S20 Rotational parameters of the ground state and vibrationally excited states (v = 1) and ratios of *a*-, *b*-, and *c*-types of C_2H_5OOH predicted with the B3LYP/aug-cc-pVTZ method

Mode	C_2H_5OOH			
	A'/*A*"	*B*'/*B*"	*C*'/*C*"	*a*-/*b*-/*c*-
ν_1	0.998	1.000	1.000	51/8/41
ν_7	0.998	1.000	1.002	83/17/0
ν_8	0.998	1.000	1.002	49/51/0
ν_9	1.004	1.002	1.000	0/0/100
ν_{10}	0.997	0.998	0.997	96/4/0
ν_{11}	0.998	0.999	0.998	20/79/1
ν_{12}	1.000	0.999	0.998	93/7/0
ν_{13}	0.999	0.999	1.001	51/17/32
ν_{14}	1.020	0.999	0.998	9/0/90
ν_{15}	0.976	0.998	1.000	18/82/0
ν_{16}	0.995	0.996	0.995	57/43/0
ν_{17}	0.998	0.996	0.997	98/0/2
ν_{18}	1.004	0.998	0.997	46/54/0
ν_{19}	0.997	0.999	0.999	17/0/82
	A" / cm^{-1}	*B*" / cm^{-1}	*C*" / cm^{-1}	
v = 0	1.0292	0.1369	0.1279	

Table S21 Rotational parameters of the ground state and vibrationally excited states (v = 1) and ratios of *a*-, *b*-, and *c*-types of C_2H_3OOH-1 and C_2H_3OOH-2 predicted with the B3LYP/aug-cc-pVTZ method

Mode	C_2H_3OOH-1				C_2H_3OOH-2			
	A'/*A*"	*B*'/*B*"	*C*'/*C*"	*a*-/*b*-/*c*-	*A*'/*A*"	*B*'/*B*"	*C*'/*C*"	*a*-/*b*-/*c*-
ν_1	0.993	1.000	1.002	37/9/55	0.997	0.999	1.001	60/2/39
ν_5	0.998	0.997	0.998	97/0/3	0.996	0.999	0.998	81/19/0
ν_6	1.002	1.001	1.000	82/17/1	1.001	1.000	1.000	58/41/0
ν_7	0.989	0.999	1.001	78/15/7	0.997	1.000	0.999	28/72/0
ν_8	1.004	1.000	0.999	0/68/32	0.999	1.002	1.000	4/96/0
ν_9	1.002	0.998	0.997	86/14/1	0.999	0.999	0.997	85/15/0
ν_{10}	0.992	1.001	1.000	57/0/42	0.998	0.999	1.000	18/21/61
ν_{11}	0.984	0.998	1.002	12/3/85	0.999	0.999	1.000	22/31/47
ν_{12}	1.013	0.997	0.995	6/4/90	0.999	0.997	0.995	90/10/0
ν_{13}	1.005	0.997	0.997	63/3/34	0.998	0.998	1.000	0/0/99
	A" / cm^{-1}	*B*" / cm^{-1}	*C*" / cm^{-1}		*A*" / cm^{-1}	*B*" / cm^{-1}	*C*" / cm^{-1}	
v = 0	1.3711	0.1522	0.1416		0.62730	0.21780	0.16320	

Table S22 Comparison of experimentally observed vibrational wavenumbers and relative IR intensities of FAA (F1) with literature values

Mode	Experiment /cm^{-1}	Literature[a] /cm^{-1}	Literature[b] /cm^{-1}	Mode Description[c]
ν_5	1810 (35)[d]	1810 (23)	1808 (s)	*iph*. C=O/C=O stretch
ν_6	1792 (94)	1792 (75)	1792 (vs)	*oph*. C=O/C=O stretch
ν_7			1442 (vw)	CH_3 deformation
ν_8			1431 (vw)	CH_2 scissor
ν_9	1378 (14)	1378 (10)	1378 (m)	CH_3 umbrella
ν_{10}			1378 (m)	CH *ip*-bend
ν_{11}	1199 (76)	1200 (67)	1200 (vs)	*oph*-CC/CO stretch
ν_{12}			1133 (m)	OC(O)C *op*-deformation
ν_{13}	1045 (100)	1045 (100)	1049 (vs)	$_{(O)}$CO stretch
ν_{14}			998 (w)	CH *op*-bend
ν_{15}			980 (m)	CH_3 wag
ν_{16}	933 (17)	930 (18)	930 (m)	*iph*-CC/CO stretch

[a]B. Behera, K. Takahashi and Y.-P. Lee, *Phys. Chem. Chem. Phys.*, 2022, **24**, 18568. [b]G. Wu, S. Shlykov, C. V. Alsenoy, H. J. Geise, E. Sluyts and B. J. van der Veken, *J. Phys. Chem.*, 1996, **100**, 11620. [c] Approximate mode description: *ip*: in-plane; *op*: out-of-plane; *iph*: in-phase; *oph*: out-of-phase. [d] Percentage integrated IR intensities relative to the most intense band (ν_{13}) at 1045 cm^{-1} are listed in parentheses.

Table S23 Experimental conditions and first-order rate coefficients k^{I} and $k^{I'}$ of the reaction CH_3CHOO + HC(O)OH in four sets of experiments

Set	Expt.	$[CH_3CHI_2]_0$ /10^{14} [a]	[HC(O)OH]$_0$ /10^{15} [a]	$[O_2]_0$ /10^{18} [a]	$[CH_3CHI]_0$ /10^{14} [a]	A_6 [b]		A_7 [b]	
						k_1^{I} /10^5 s^{-1}	$k_1^{I'}$ /10^5 s^{-1}	k_1^{I} /10^5 s^{-1}	$k_1^{I'}$ /10^5 s^{-1}
1	1	12.6	0.35	1.3	3.3	1.56 (0.19)	1.23 (0.09)	1.12 (0.19)	0.80 (0.09)
	2	12.6	1.21	1.3	3.1	2.95 (0.16)	2.59 (0.13)	2.46 (0.16)	2.13 (0.25)
	3	12.6	1.47	1.3	3.6	3.60 (0.26)	3.18 (0.18)	3.12 (0.26)	2.75 (0.24)
	4	12.6	1.91	1.3	2.9	4.33 (0.36)	3.98 (0.21)	4.36 (0.36)	4.03 (0.36)
	5	12.6	2.69	1.3	2.9	6.12 (0.40)	5.83 (0.30)	5.92 (0.40)	5.64 (0.52)
	6	12.6	2.93	1.3	2.8	6.72 (0.42)	6.45 (0.28)	6.77 (0.42)	6.51 (0.56)
2	7	19.4	0.95	1.3	5.9	2.20 (0.10)	1.67 (0.05)	1.87 (0.10)	1.38 (0.11)
	8	19.4	1.04	1.3	5.2	2.32 (0.09)	1.87 (0.11)	2.06 (0.09)	1.61 (0.18)
	9	19.4	1.75	1.3	5.5	3.58 (0.13)	3.22 (0.13)	3.60 (0.13)	3.07 (0.22)
	10	19.4	2.27	1.3	6.2	4.75 (0.23)	4.19 (0.15)	4.45 (0.23)	3.86 (0.27)
	11	19.4	2.95	1.3	4.9	6.25 (0.36)	5.81 (0.23)	5.90 (0.36)	5.49 (0.42)
	12	19.4	3.73	1.3	5.0	8.05 (0.52)	7.75 (0.28)	8.84 (0.52)	7.66 (0.44)
3	13	16.2	0.43	1.3	5.1	1.80 (0.14)	1.34 (0.09)	1.51 (0.14)	1.14 (0.10)
	14	16.2	0.95	1.3	4.5	2.28 (0.09)	1.86 (0.10)	1.82 (0.09)	1.40 (0.10)
	15	16.2	1.71	1.3	4.8	3.84 (0.17)	3.36 (0.13)	3.50 (0.17)	3.04 (0.13)
	16	16.2	2.27	1.3	4.6	5.23 (0.39)	4.79 (0.20)	4.80 (0.39)	4.44 (0.20)
	17	16.2	2.86	1.3	4.6	6.45 (0.54)	6.02 (0.21)	6.28 (0.54)	5.85 (0.28)
	18	16.2	3.72	1.3	4.6	8.21 (0.83)	7.90 (0.32)	9.10 (0.83)	9.29 (0.50)
4	19	15.6	0.47	2.6	1.8	0.78 (0.18)	1.09 (0.12)	1.22 (0.18)	1.00 (0.15)
	20	15.6	0.80	2.6	1.5	1.93 (0.24)	1.69 (0.21)	1.71 (0.24)	1.53 (0.16)
	21	15.6	1.71	2.6	1.6	4.18 (0.08)	3.82 (0.30)	*5.17 (0.64)*	*4.79 (0.48)*
	22	15.6	2.30	2.6	1.2	5.39 (0.17)	5.02 (0.45)	4.95 (0.17)	4.63 (0.47)
	23	15.6	2.83	2.6	2.4	6.16 (0.19)	5.66 (0.44)	6.67 (0.19)	6.21 (0.49)
	24	15.6	3.44	2.6	2.7	8.97 (0.54)	8.32 (0.75)	7.75 (0.54)	7.23 (0.50)

[a] in unit of molecule cm^{-3}. [b] Bands A_6 and A_7 are integrated over 1150−1175 cm^{-1} and 1180−1210 cm^{-1}, respectively. k_1^{I} and $k_1^{I'}$ are rate coefficients obtained from exponential fit and model fit, respectively. The standard deviations in fitting are listed in parentheses. Outlier data points excluded in the fitting (Fig. 12) are listed in italic.

Table S24 The kinetic model employed in fitting the temporal profiles of bands A_6 and A_7 in the reaction $CH_3CHOO + HC(O)OH$

	Reaction	Rate coefficient [a]		Reference
		40 Torr	80 Torr	
1	$CH_3CHI + O_2 \rightarrow CH_3CHOO + I$	6.1×10^{-12}	5.5×10^{-12}	[b]
2	$CH_3CHI + O_2 \rightarrow CH_3CHIOO$	0.7×10^{-12}	1.3×10^{-12}	[b]
3	$CH_3CHI + O_2 \rightarrow$ other	1.8×10^{-12}	1.8×10^{-12}	[b]
4	$2\ CH_3CHOO \rightarrow 2\ CH_3CHO + O_2$	1.6×10^{-10}		[c]
5	$CH_3CHIOO + CH_3CHOO \rightarrow$ other	1.0×10^{-10}		[d]
6	$CH_3CHOO + HC(O)OH \rightarrow$ HPEF	$k^{I} = k_3 \times [HC(O)OH]_0$, fitted		
7	HPEF $\rightarrow$ FAA	1420 s^{-1}		This work

[a] Rate coefficient in cm^3 $molecule^{-1}$ s^{-1}, unless otherwise specified. [b] The total rate coefficient 8.6×10^{-12} cm^3 $molecule^{-1}$ s^{-1} was taken from Howes et al., *Phys. Chem. Chem. Phys*., 2018, **20**, 22218; a value of 8.0×10^{-12} cm^3 $molecule^{-1}$ s^{-1} was reported by Sheps et al., *Phys. Chem. Chem. Phys*., 2014, **16**, 26701. The branching of $CH_3CHI + O_2$ was based on our unpublished work. [c] From Luo et al. *J. Phys. Chem. Lett.*, 2018, **9**, 4391. [d] Rate coefficient unknow; a rate of 1.0×10^{-10} cm^3 $molecule^{-1}$ s^{-1} similar to $CH_2IOO + CH_2OO$ was assumed.

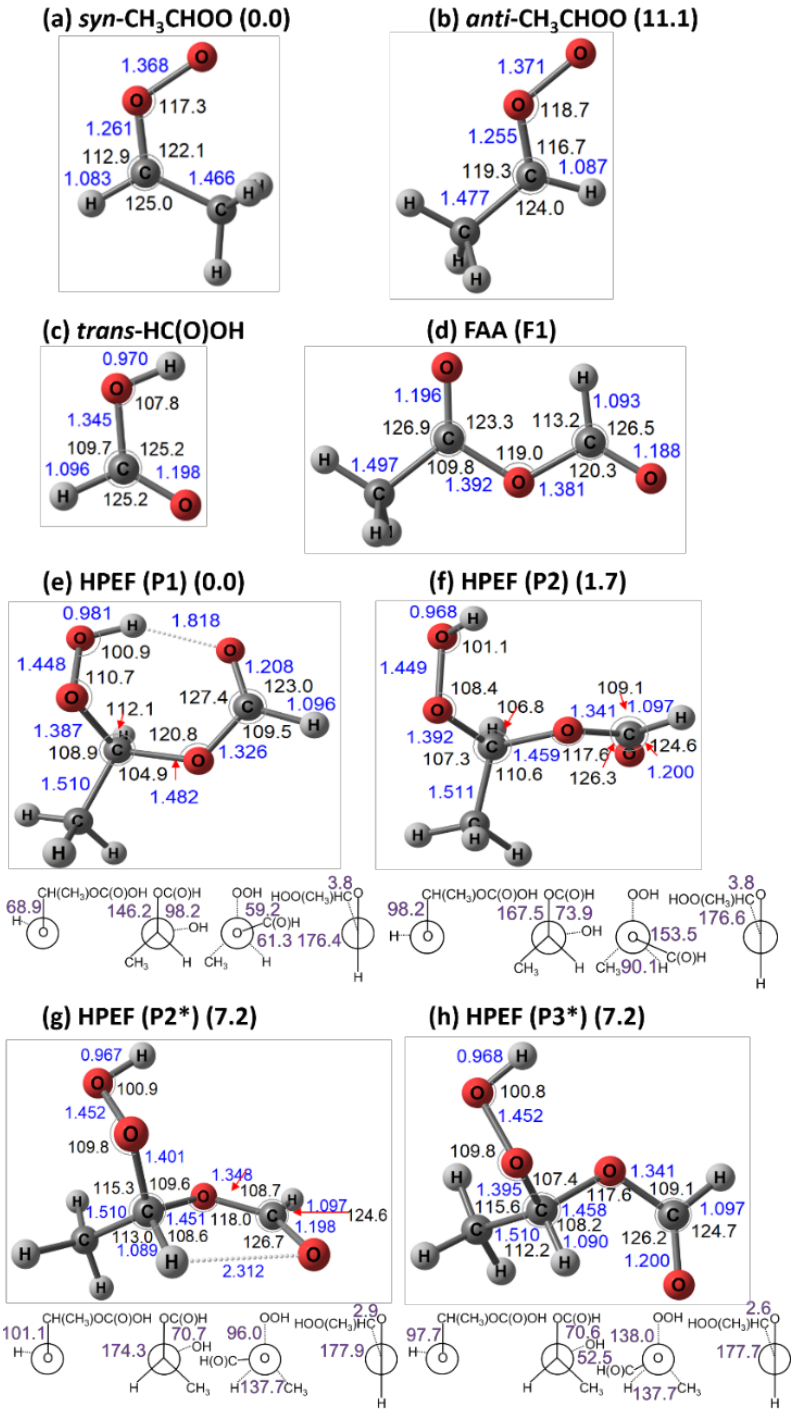

Fig. S1 Geometries of species observed in this work. (a) *anti*-CH_3CHOO, (b) *syn*-CH_3CHOO, (c) *trans*-HC(O)OH, (d) formic acetic anhydride (FAA, F1), (c) hydroperoxyethyl formate (HPEF, P1), (d) HPEF (P2), (e) HPEF (P2*), and (e) HPEF (P3*). The structures were computed with the B3LYP/aug-cc-pVTZ method. Relative energies (in kJ mol^{-1}) among conformers are listed in parentheses; energies were calculated with the CCSD(T) method at the geometries optimized with the B3LYP/aug-cc-pVTZ method and corrected for vibrational zero-point energy.

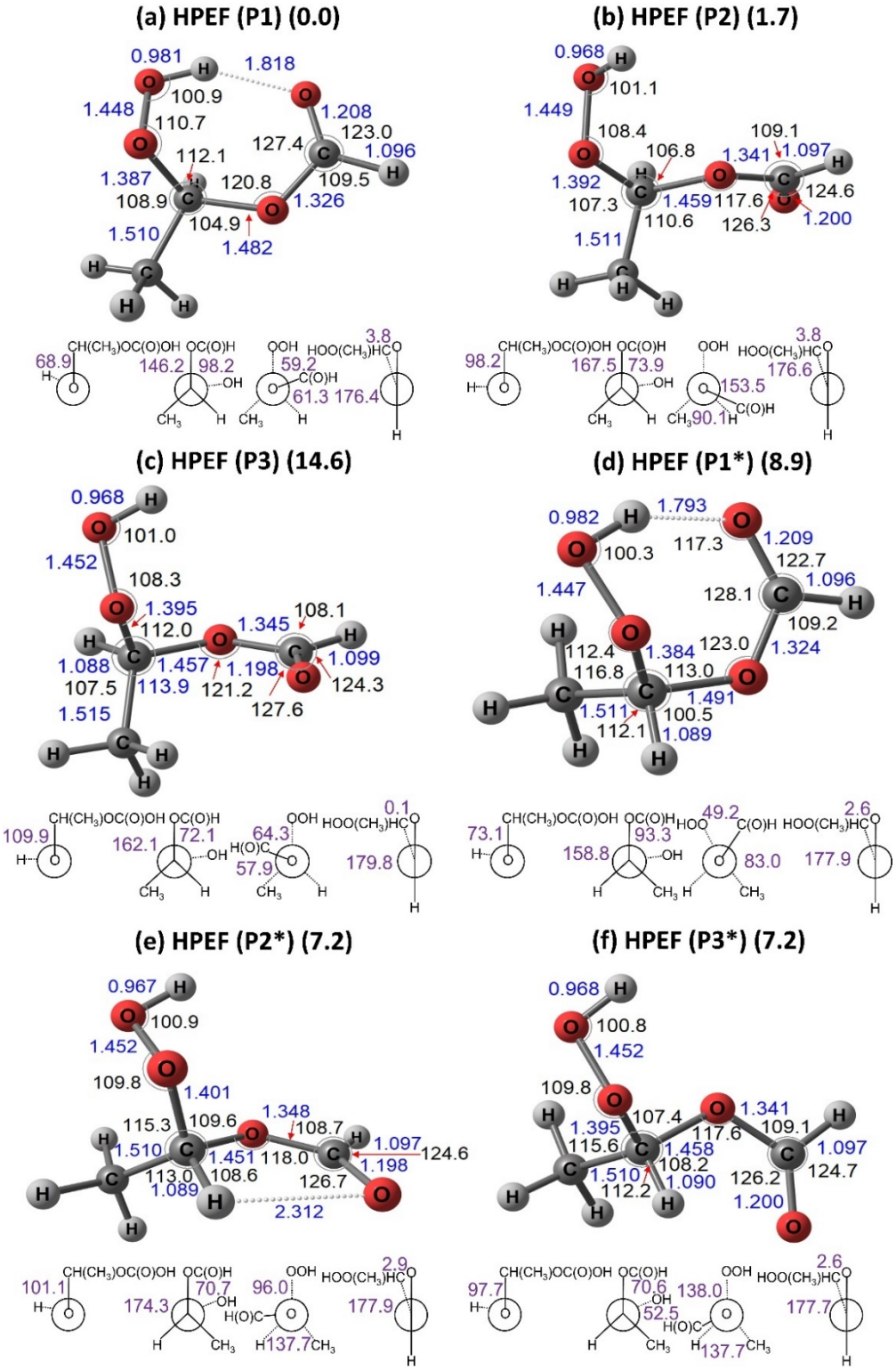

Fig. S2 Geometries of possible conformers of hydroperoxyethyl formate (HPEF) in the reaction of CH_3CHOO + HC(O)OH. Conformers of HPEF: (a) P1, (b) P2, (c) P3, (d) P1*, (e) P2*, (f) P3*. The structures were calculated with the B3LYP/aug-cc-pVTZ method and the energies were calculated with the CCSD(T)/aug-cc-pVTZ//B3LYP/aug-cc-PVTZ method with zero-point vibrational energy at the B3LYP level corrected. Relative energy with respect to the least-energy conformer P1 is presented in parentheses. Bond distances (blue) are in Å and bond angles (in black) are in degree.

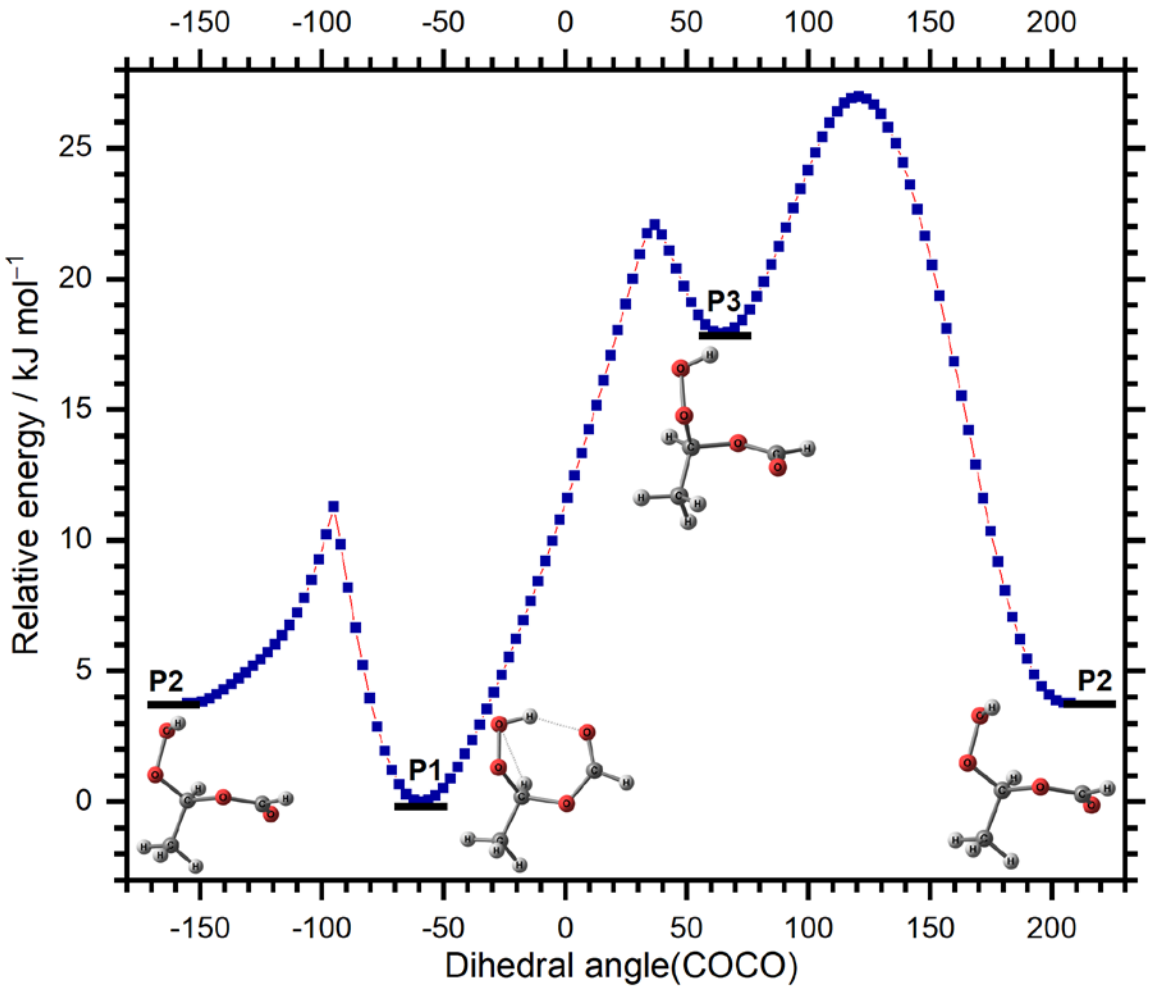

Fig. S3 Potential-energy curve calculated as a function of the COCO dihedral angle for the interconversion among conformers of HPEF (P1–P3) produced from *anti*-CH_3CHOO + HC(O)OH. The energies are calculated with the B3LYP/aug-cc-pVTZ methods. The zero energy is set as that of the most stable conformer P1.

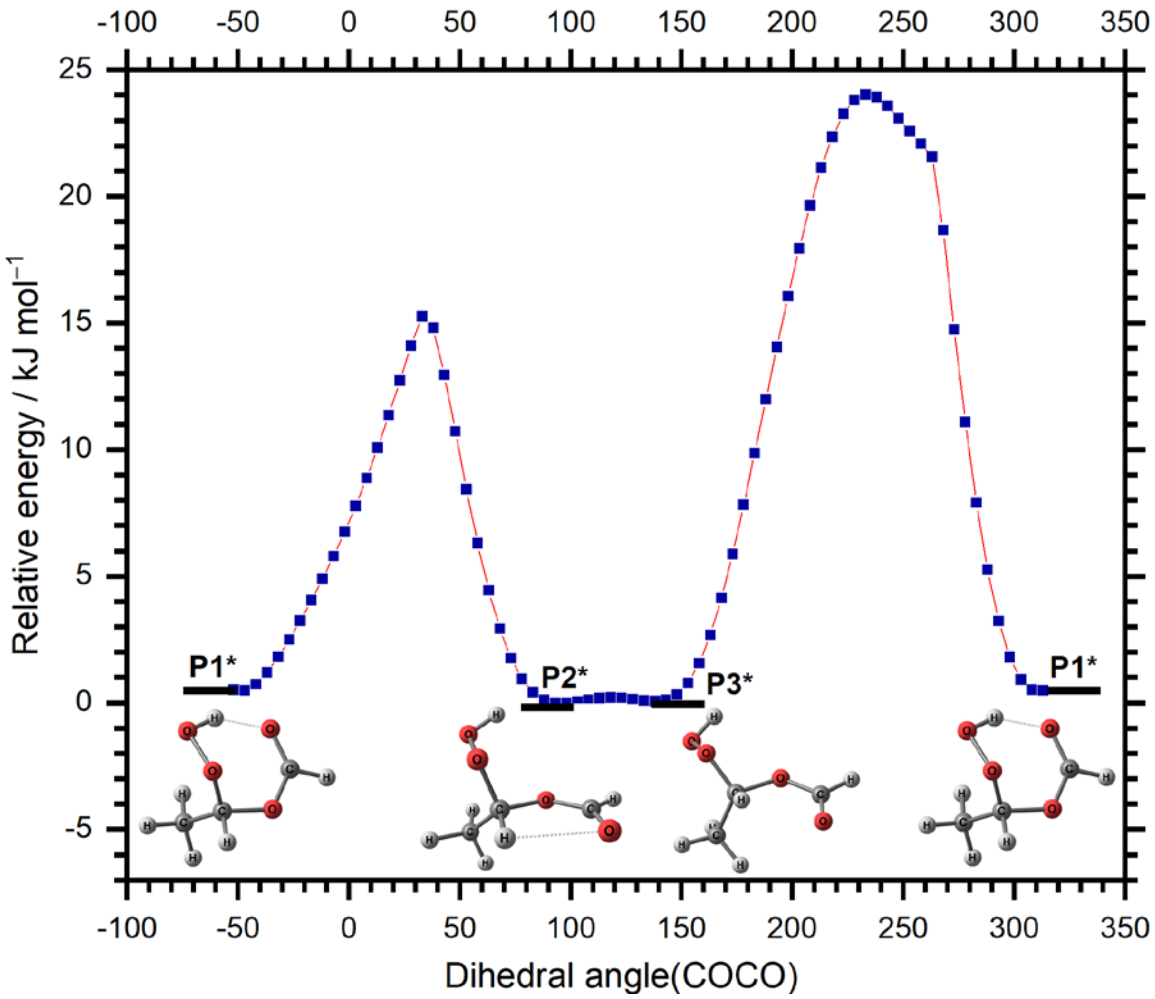

Fig. S4 Potential-energy curve calculated as a function of the COCO dihedral angle for the interconversion among conformers of HPEF (P1*–P3*) produced from *syn*-CH_3CHOO + HC(O)OH. The energies are calculated with the B3LYP/aug-cc-pVTZ methods. The zero energy is set as that of the most stable conformer P2*.

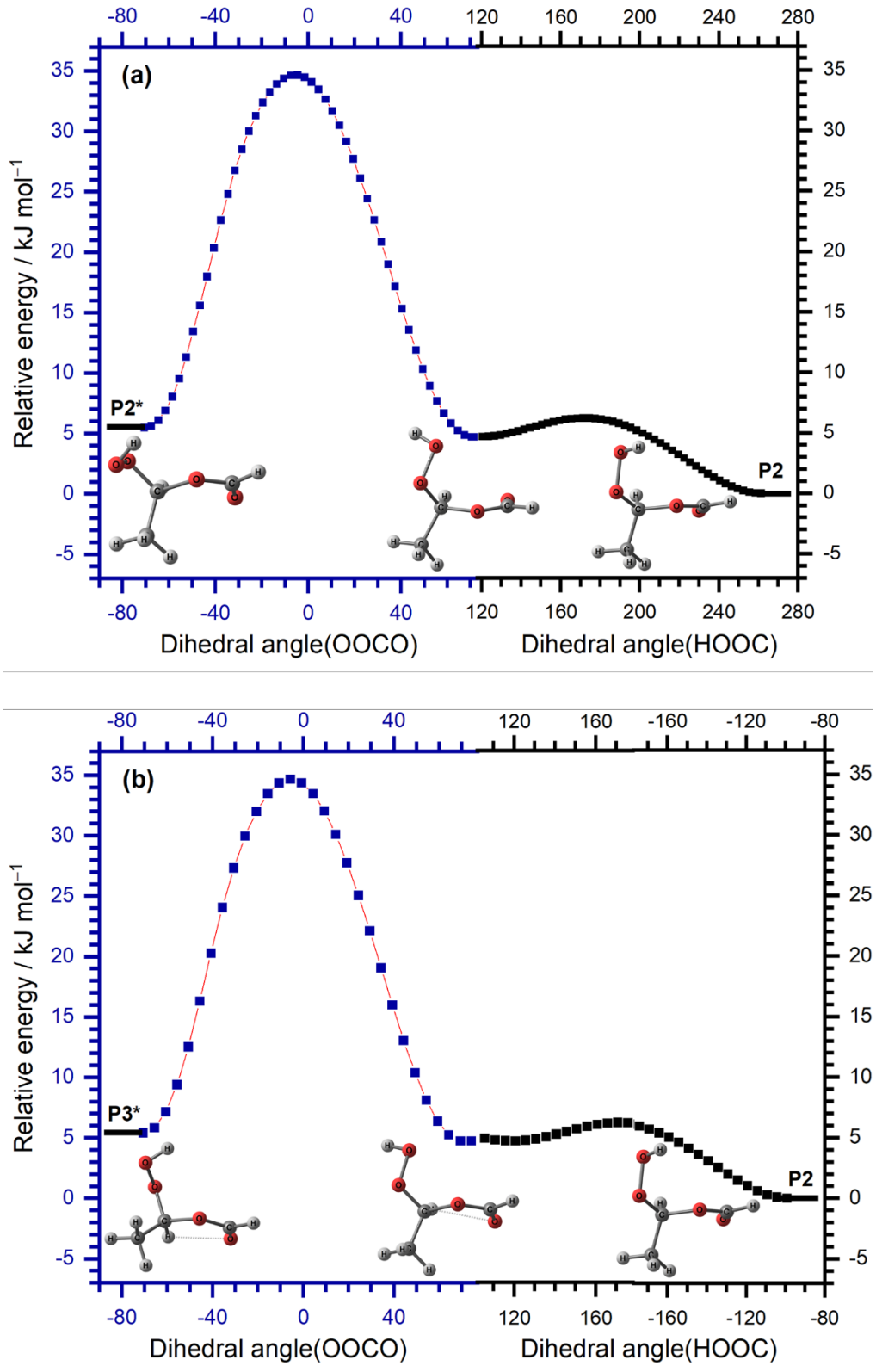

Fig. S5 Potential-energy curves calculated for the interconversion HPEF conformers between P2*/P3* and P2. (a) P2* to P2, and (b) P3* to P2. We connected two scans to present the interconversion in the same figure. The scan for OOCO, and HOOC dihedral angles is presented in blue, and black color, respectively. The energies are calculated with the B3LYP/aug-cc-pVTZ methods. The least energy conformer P2 energy is set as zero.

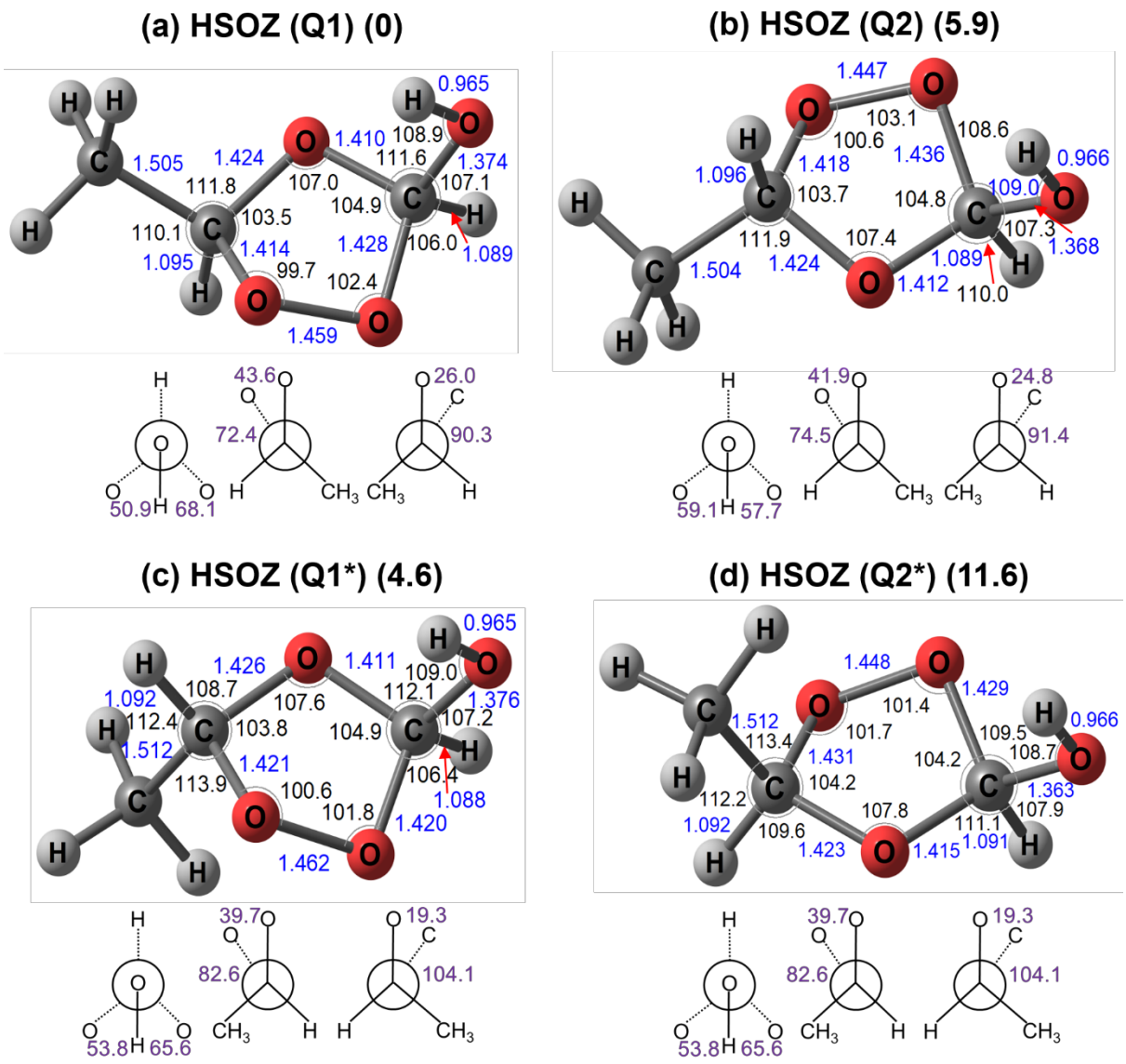

Fig. S6 Geometries of possible conformers of hydroxylated secondary ozonide (HSOZ) produced in the reaction of CH_3CHOO + HC(O)OH. Conformers of HSOZ: (a) Q1, (b) Q2, (c) Q1*, and (d) Q2*. The structures were calculated with the B3LYP/aug-cc-pVTZ method and the energies were calculated with the CCSD(T)/aug-cc-pVTZ//B3LYP/aug-cc-PVTZ method with zero-point vibrational energy at the B3LYP level corrected. Relative energy with respect to the least-energy conformer Q1 is presented in parentheses. Bond distances (blue) are in Å and bond angles (in black) are in degree.

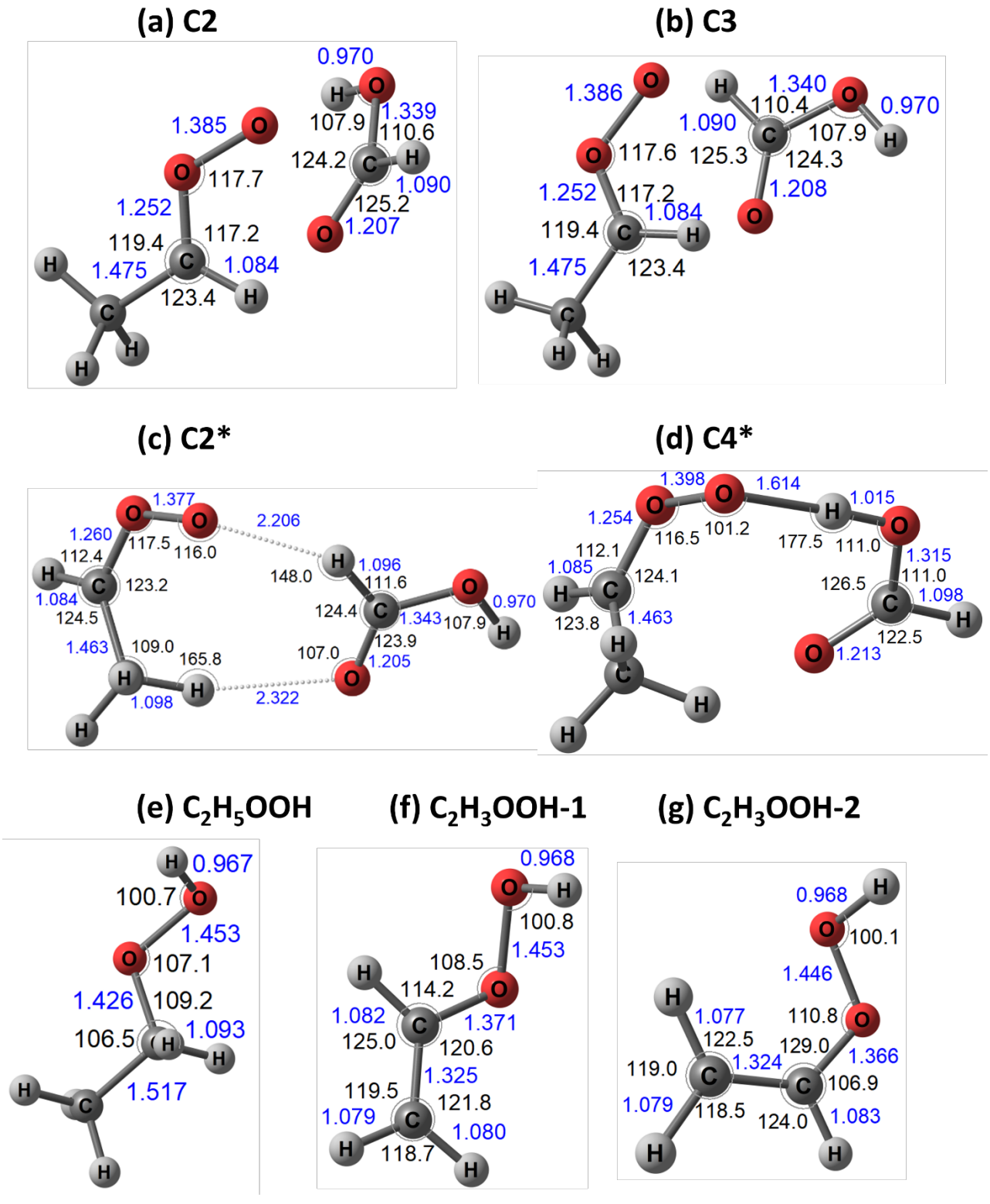

Fig. S7 Geometries of pre-reactive complexes and products other than dehydrated products in the reaction of CH_3CHOO + HC(O)OH. Complexes and products: (a) C2, (b) C3, (c) C2*, (d) C4*, (e) C_2H_5OH, (f) C_2H_3OOH-1, and (d) C_2H_3OOH-2. The structures were calculated with the B3LYP/aug-cc-pVTZ method. Bond distances (blue) are in Å and bond angles (in black) are in degrees.

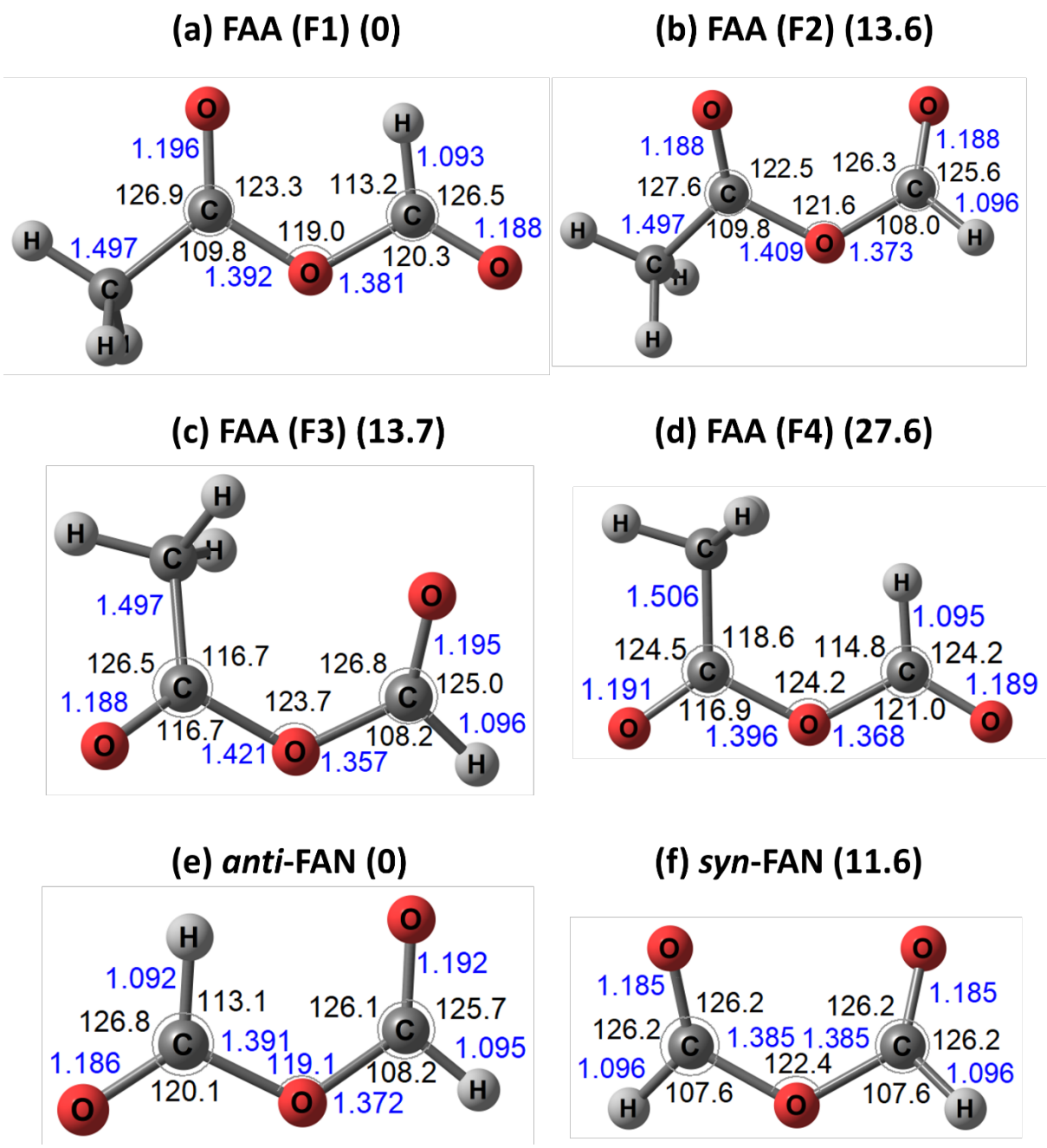

Fig. S8 Geometries of conformers of formic acetic anhydride (FAA) and formic anhydride (FAN) produced in the reaction of CH_3CHOO + HC(O)OH. Conformers of FAA: (a) F1, (b) F2, (c) F3, and (d) F4. Conformers of FAN: (e) *anti*-FAN, and (f) *syn*-FAN. The structures were calculated with the B3LYP/aug-cc-pVTZ method and the energies were calculated with the CCSD(T)/aug-cc-pVTZ//B3LYP/aug-cc-PVTZ method with zero-point vibrational energy at the B3LYP level corrected. Relative energy with respect to the least-energy conformer is presented in parentheses. Bond distances (blue) are in Å and bond angles (in black) are in degree.

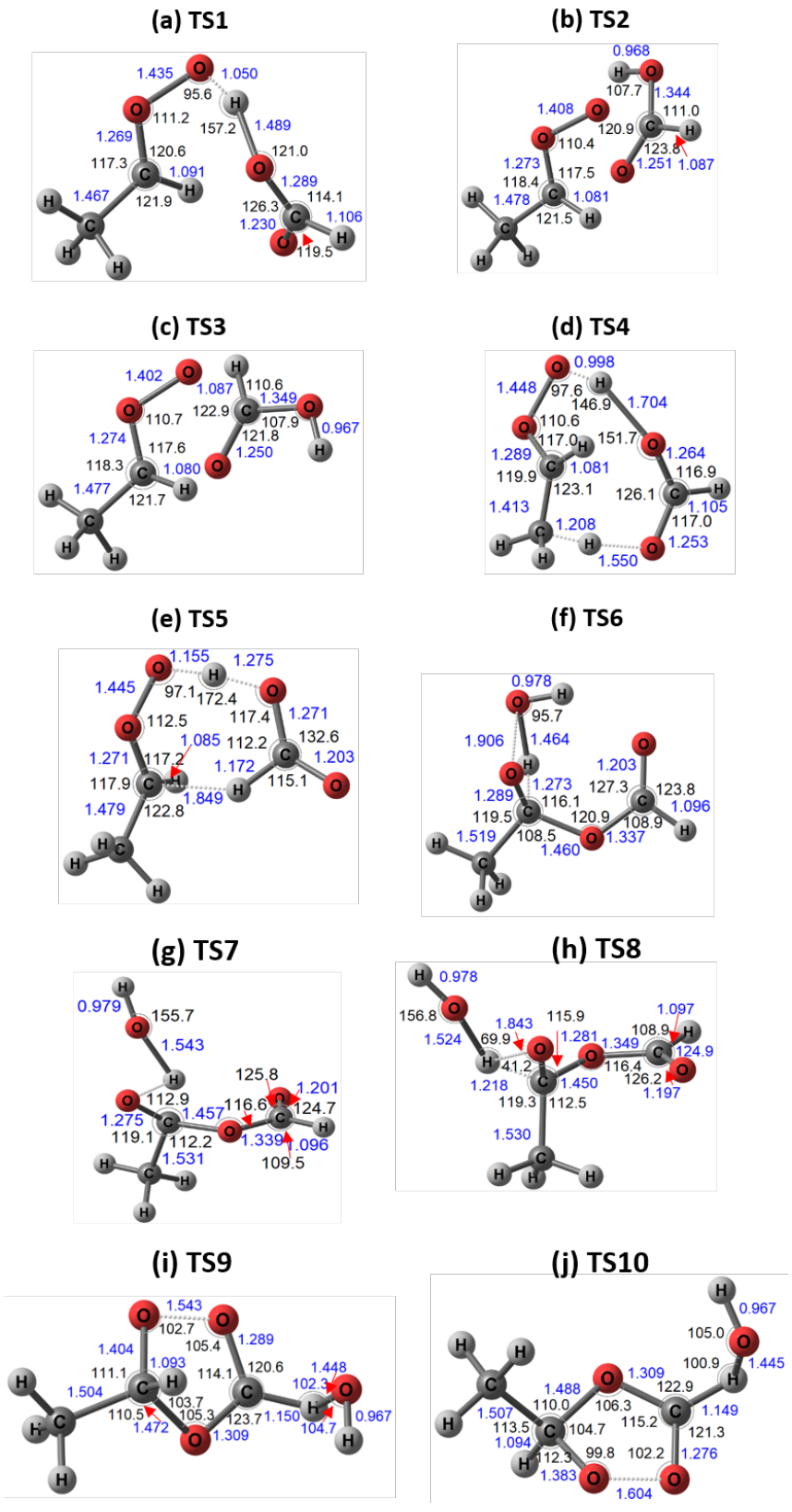

Fig. S9 Geometries of transition states in the reaction of *anti*-CH_3CHOO + HC(O)OH. The structures were calculated with the B3LYP/aug-cc-pVTZ method. Bond distances (blue) are in Å and bond angles (in black) are in degree.

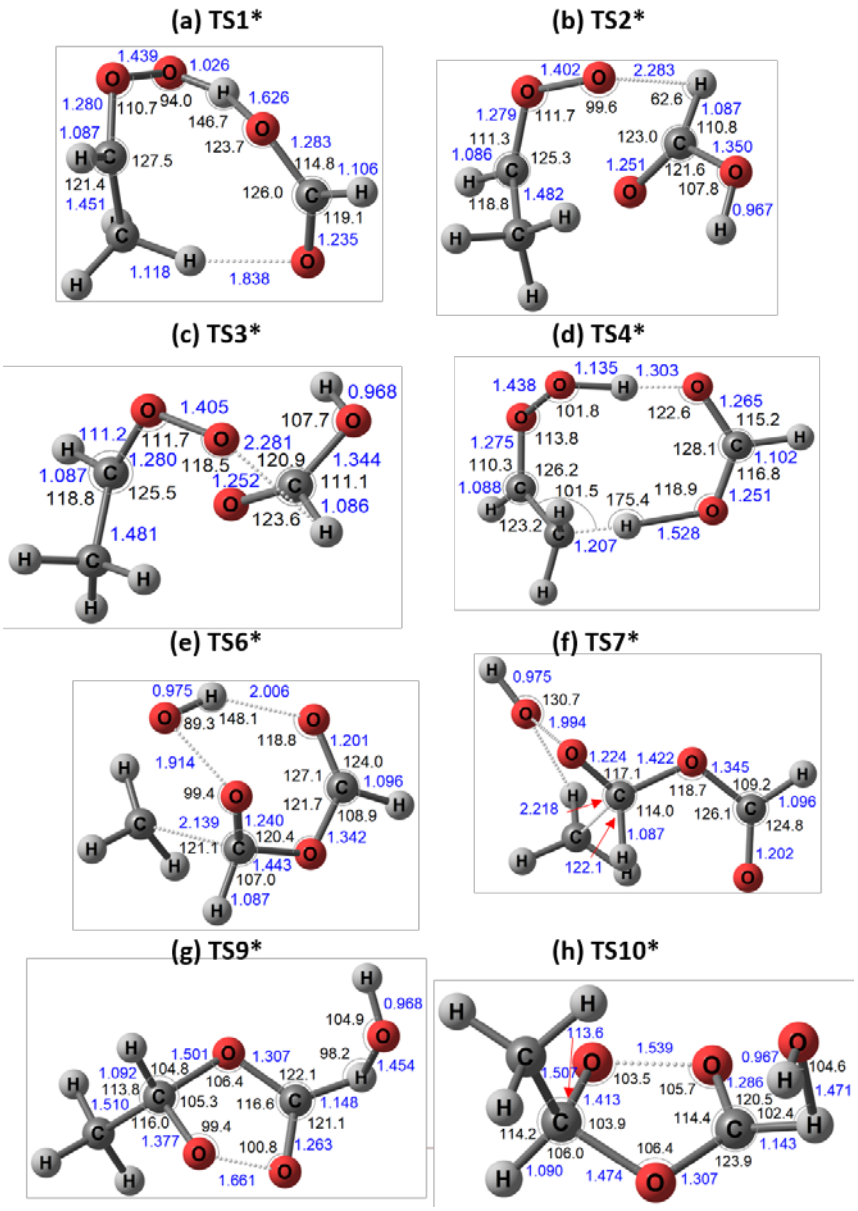

Fig. S10 Geometries of transition states in the reaction of *syn*-CH_3CHOO + HC(O)OH. The structures were calculated with the B3LYP/aug-cc-pVTZ method. Bond distances (blue) are in Å and bond angles (in black) are in degree.

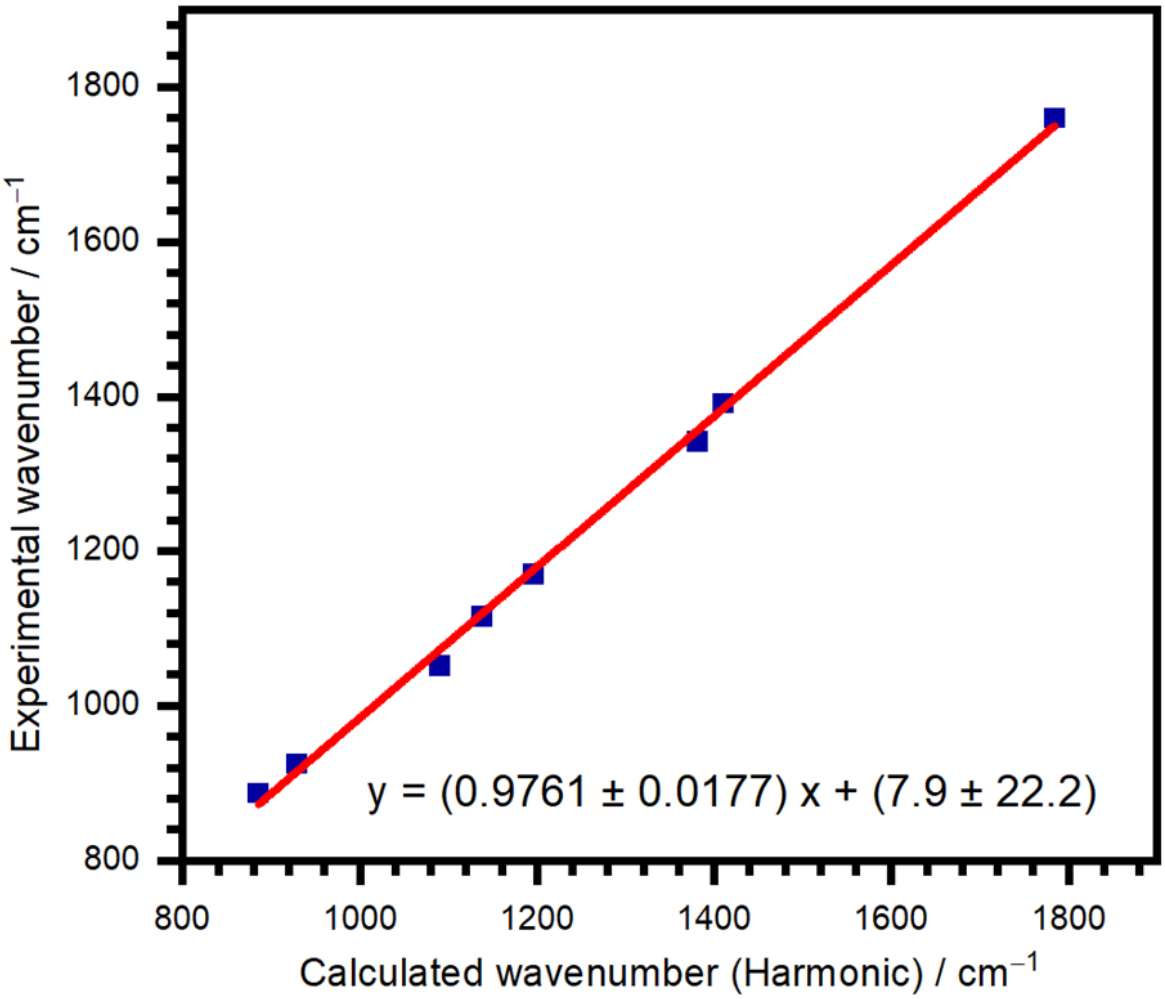

Fig. S11 Linear fit of experimental wavenumbers vs. calculated harmonic vibrational wavenumbers of hydroperoxylmethyl formate (HPMF). Data taken from C.-A. Chung, J. W. Su and Y.-P. Lee, *Phys. Chem. Chem. Phys.*, 2019, **21**, 21445. The linear equation obtained on fitting the data is $y = (0.9761 \pm 0.0177)\ x + (7.9 \pm 22.2)$; y is the scaled wavenumber and x is the calculated harmonic vibrational wavenumber.

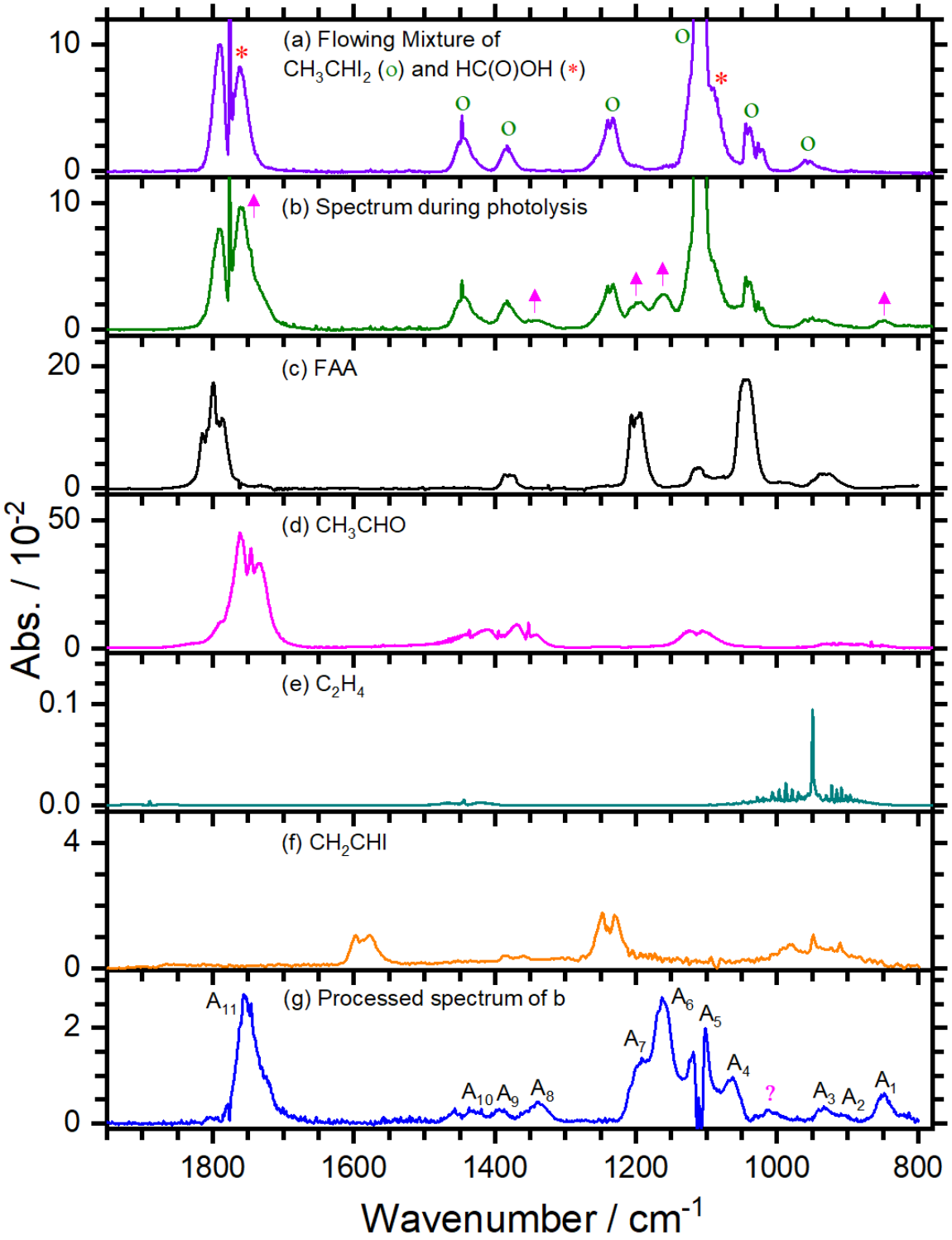

Fig. S12 Observed spectra in region 770–1950 cm^{-1} during photolysis at 308 nm (5 Hz, 180 mJ $pulse^{-1}$) of a flowing mixture of $CH_3CHI_2/O_2/HC(O)OH$ (0.064/53.9/0.020, P_T = 54.0 torr) recorded with continuous scan. (a) Spectrum before photolysis. Features of CH_3CHI_2 and HC(O)OH are denoted with green circles and red asterisks, respectively. (b) Spectrum during photolysis. New features are indicated by pink arrows. Reference spectra of formic acetic anhydride FAA (c), CH_3CHO (d), C_2H_4 (e), and CH_2CHI (f). (g) Processed spectra in (b), with feature of HC(O)OH, CH_3CHI_2, FAA, CH_3CHO, C_2H_4, and CH_2CHI removed. Features in group A are indicated. The instrumental resolution is 1 cm^{-1}.

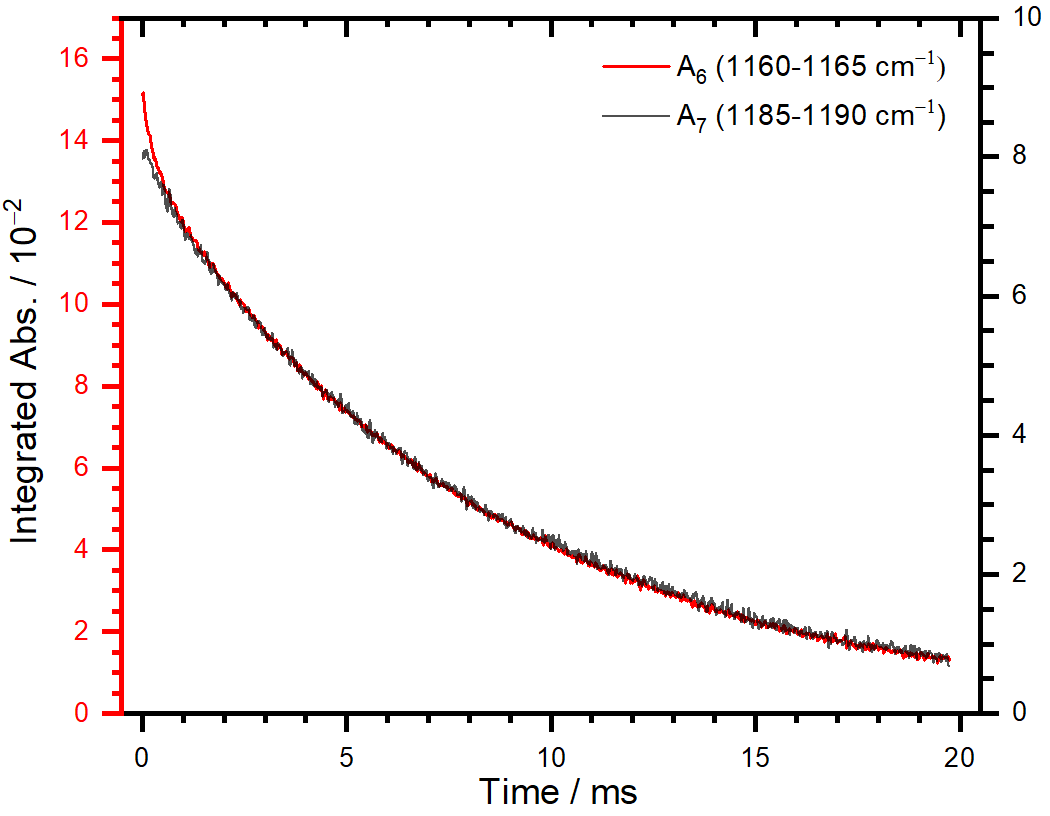

Fig. S13 Comparison of temporal evolution of bands A_6 and A_7. The traces of bands A_6 (red), and A_7 (black) were obtained on integrating over the regions 1160–1165 and 1185–1190 cm^{-1}, respectively. The left ordinate and right ordinate are for bands A_6 and A_7, respectively.

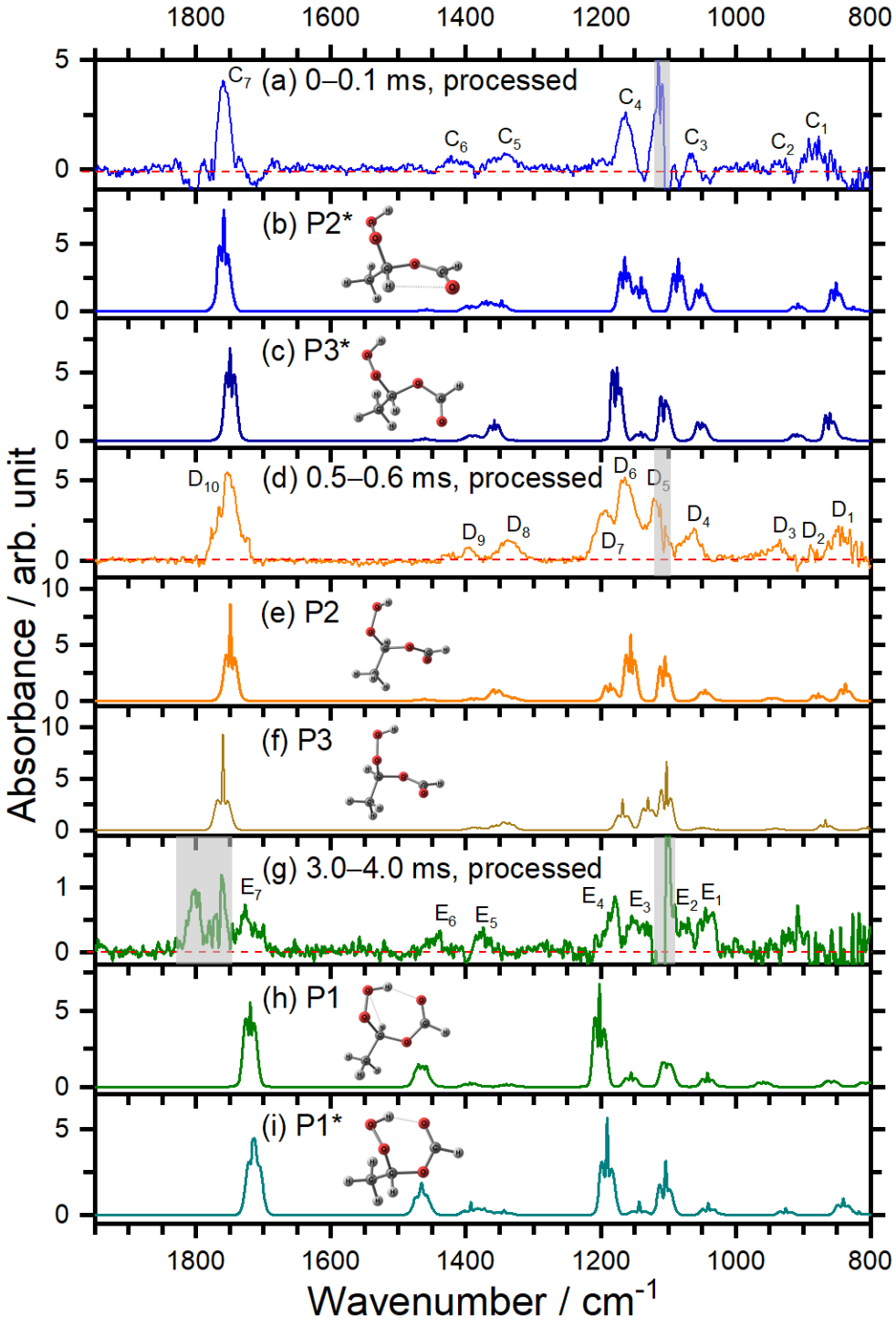

Fig. S14 Comparison of observed spectra in groups C, D, and E with simulated IR spectra of conformers of HPEF. (a) Processed spectrum of group C, reproduced from Fig. 8e. Simulated IR spectra of HPEF (P2*) (b) and HPEF (P3*) (c). (d) Processed spectrum of group D, reproduced from Fig. 8f. Simulated IR spectra of HPEF (P2) (e) and HPEF (P3) (f). (g) Processed spectrum of group E, reproduced from Fig. 8g. Simulated IR spectra of HPEF (P1) (h) and HPEF (P1*) (i). Spectra were simulated according to scaled vibrational wavenumbers, harmonic IR intensities, rotational parameters, and type ratios predicted with the B3LYP/aug-cc-pVTZ method. The regions of interference from absorption of CH_3CHI_2 and HC(O)OH are shaded gray. The instrumental resolution is 2 cm^{-1}.

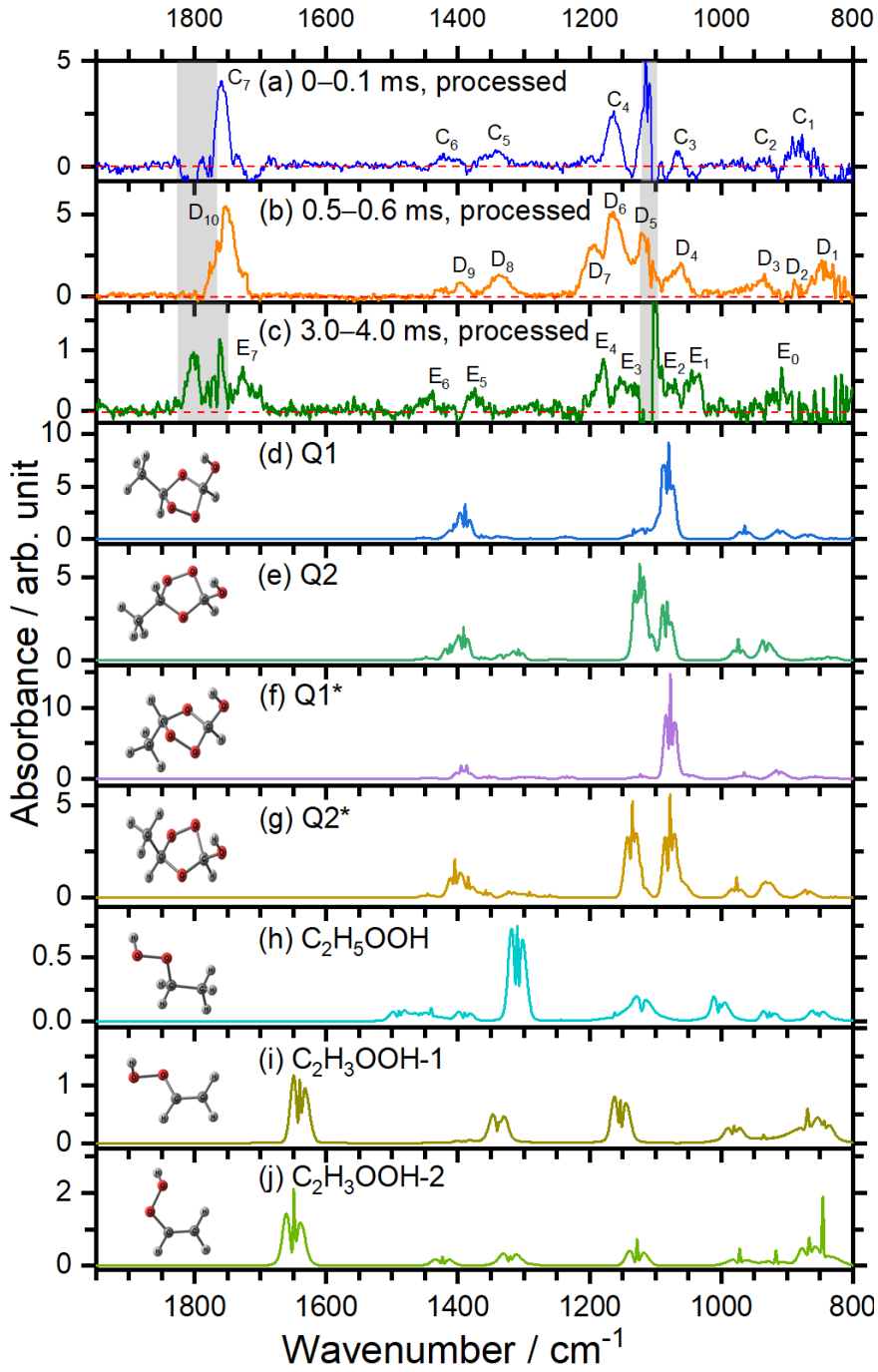

Fig. S15 Comparison of the observed spectra in groups C, D, and E with simulated IR spectra of conformers of HSOZ (Q1, Q2, Q1*, and Q2*), C_2H_5OOH, C_2H_3OOH-1, and C_2H_3OOH-2. (a) Processed spectrum of group C, reproduced from Fig. 8e. (b) Processed spectrum of group D, reproduced from Fig. 8f. (c) Processed spectrum of group E, reproduced from Fig. 8g. (d)−(j) Simulated IR spectra of HSOZ (Q1), HSOZ (Q2), HSOZ (Q1*), HSOZ (Q2*), C_2H_5OOH, C_2H_3OOH-1, and C_2H_3OOH-2 according to anharmonic vibrational wavenumbers and harmonic IR intensities predicted with the B3LYP/aug-cc-pVTZ method. The regions of interference from absorption of CH_3CHI_2 and HC(O)OH are shaded gray. The instrumental resolution is 2 cm^{-1}.

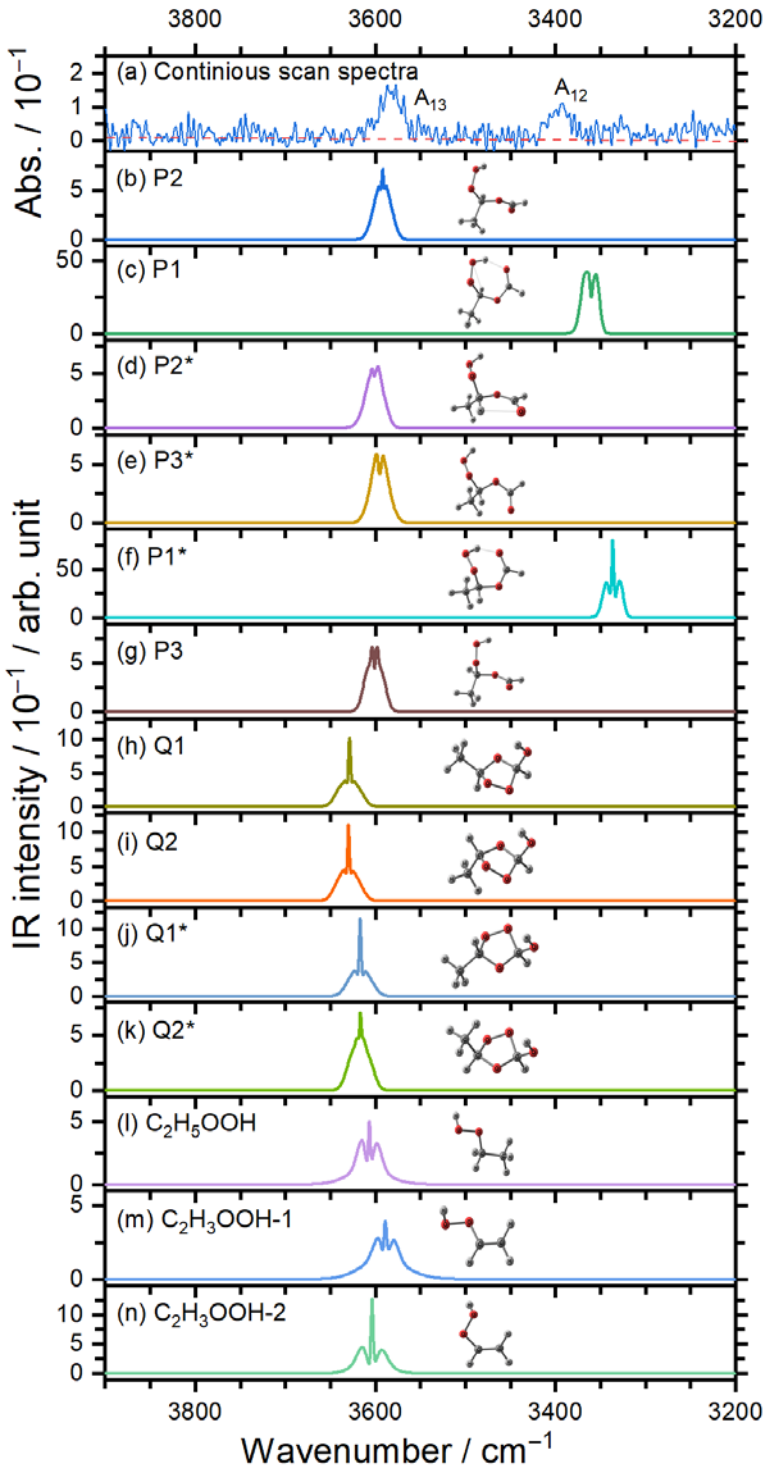

Fig. S16 Comparison of bands A12 and A13 observed in region 3200–3900 cm^{-1} with simulated IR spectra of possible conformers of HPEF (P1–P3, P1*–P3*), HSOZ (Q1–Q2, Q1*–Q2*), C_2H_5OOH, C_2H_3OOH-1, and C_2H_3OOH-2. (a) Flow cell experiment spectra reproduced from Fig. 6c. Simulated IR spectra of (b) HPEF (P2), (c) HPEF (P1), (d) HPEF (P2*), (e) HPEF (P3*), (f) HPEF (P1*), (g) HPEF (P3), (h) HSOZ (Q1), (i) HSOZ (Q2), (j) HSOZ (Q1*), (k) HSOZ (Q2*), (l) C_2H_5OOH, (m) C_2H_3OOH-1, and (n) C_2H_3OOH-2 according to scaled harmonic vibrational wavenumbers and harmonic IR intensities predicted with the B3LYP/aug-cc-pVTZ method. The instrumental resolution is 2 cm^{-1}.

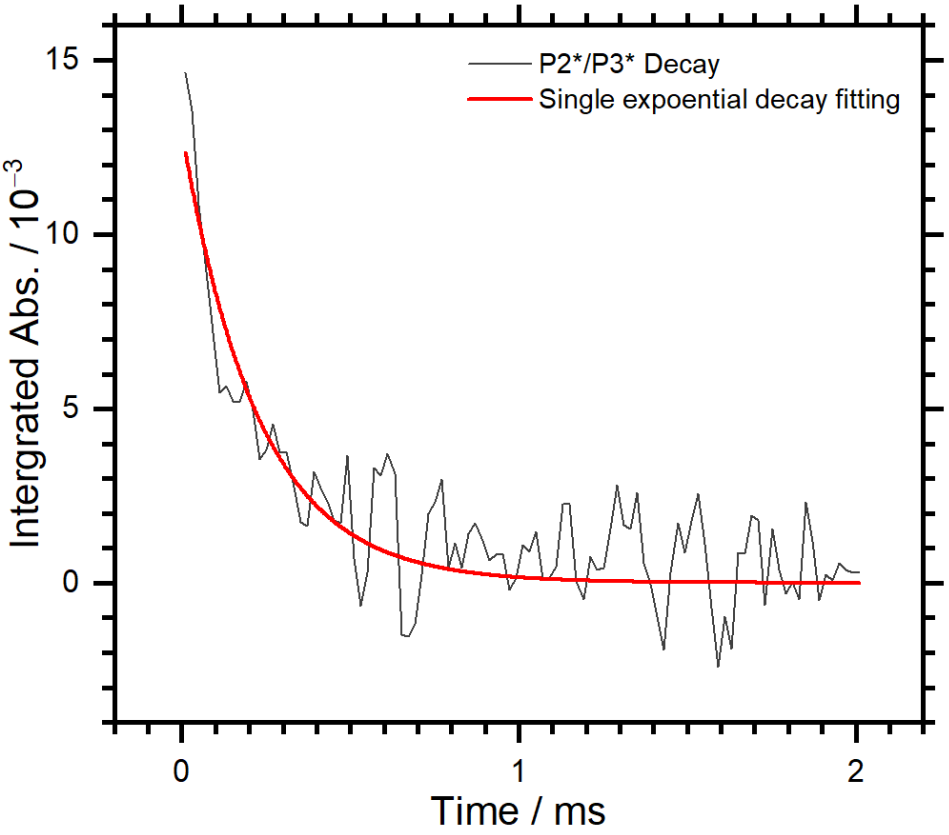

Fig. S17 Exponential fit of the decay of P2*/P3*. The temporal profile was obtained on subtracting 1.73 times the integrated absorbance of band A_7 (integrated over 1180–1210 cm^{-1}) from that of band A_6 (integrated over 1150–1175 cm^{-1}). The red line represents a single exponential fit with a decay rate coefficient (4430 ± 390) s^{-1}.

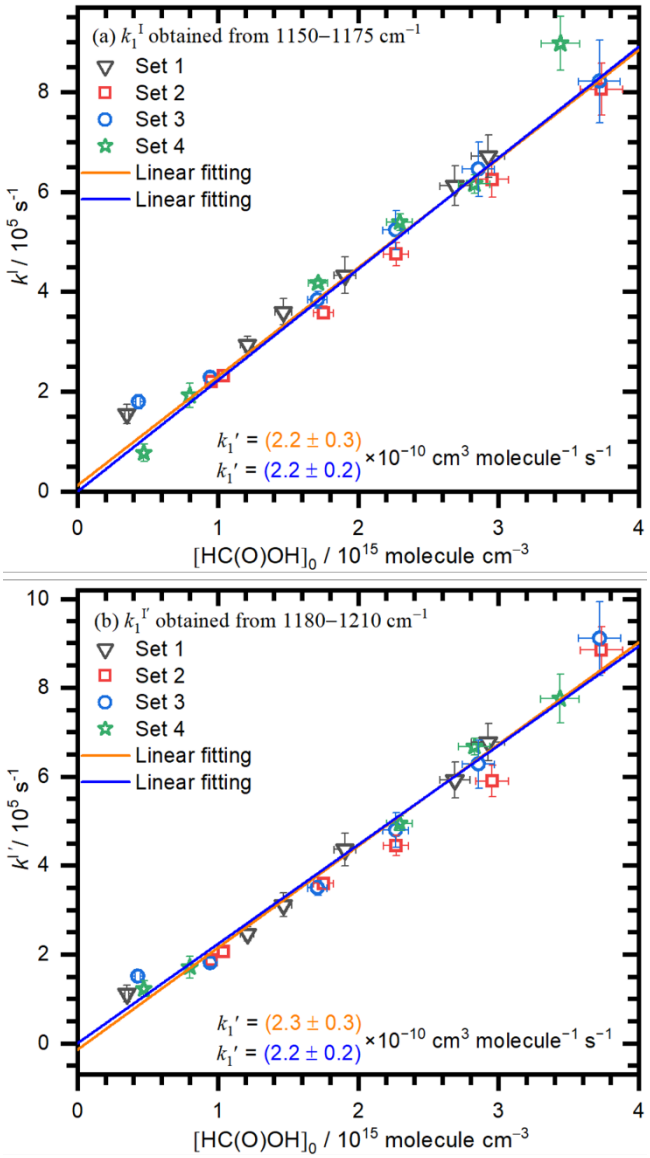

Fig. S18 Fitted first-order rate coefficients k_1^I (A_6) and k_1^I (A_7) as a function of $[HC(O)OH]_0$. (a) k_1^I (A_6) and (b) k_1^I (A_7) derived from the single exponential-rise fitting for the reaction $CH_3CHOO + HC(O)OH \rightarrow$ HPEF. Bands A_6 and A_7 were integrated over regions 1150–1175 cm^{-1} and 1180–1210 cm^{-1}, respectively. The orange line represents a linear fit to $y = ax + b$ and the slope represents bimolecular rate coefficient k_1; $k_1'(A_6) = (2.2 \pm 0.3)\times10^{-10}$ and $k_1(A_7) = (2.3 \pm 0.3)\times10^{-10}$ cm^3 molecule^{-1} s^{-1}. The blue line represents a linear fit to $y = ax$; $k_1(A_6) = (2.2 \pm 0.2)\times10^{-10}$ and $k_1(A_7) = (2.2 \pm 0.2)\times10^{-10}$ cm^3 molecule^{-1} s^{-1}.

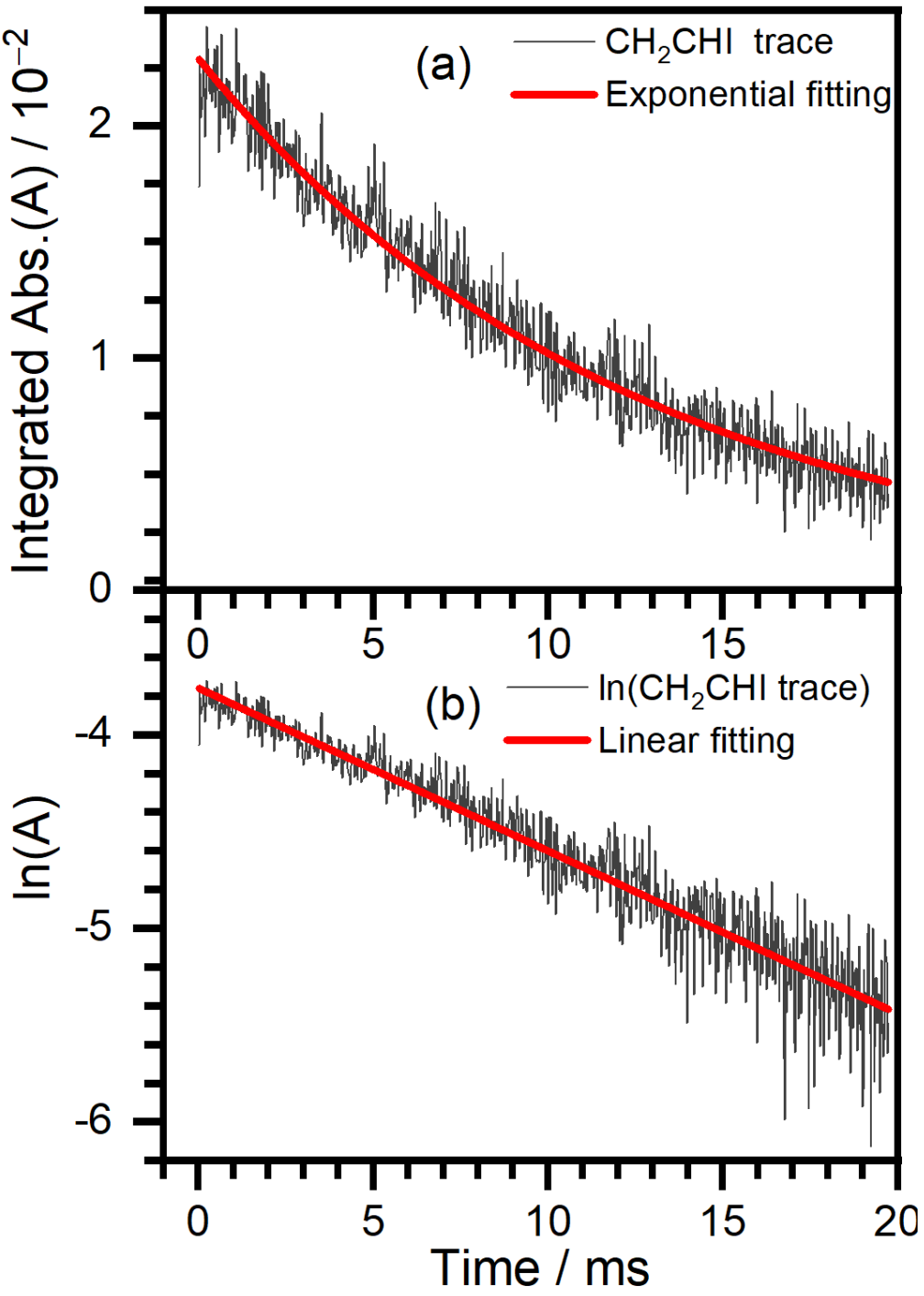

Fig. S19 Temporal profiles for the decay of CH_2CHI due to pumping. The solid red lines represent fitted temporal profiles. The data was obtained on integrating over the region 1585−1610 cm^{-1} at temporal resolution 20 μs. (a) Integrated absorbance A of CH_2CHI and the single exponential fitting, (b) semi-logarithmic plot of integrated absorbance A of CH_2CHI vs. time and the linear fitting.

References

[1] N. U. M. Howes, Z. S. Mir, M. A. Blitz, S. Hardman, T. R. Lewis, D. Stone and P. W. Seakins, *Phys. Chem. Chem. Phys*., 2018, **20**, 22218

[2] L. Sheps, A. M. Scully and K. Au, *Phys. Chem. Chem. Phys*., 2014, **16**, 26701

[3] W.-L. Ting, C.-H. Chang, Y.-F. Lee, H. Matsui, Y.-P. Lee and J. J.-M. Lin, *J. Chem. Phys.*, 2014, **141**, 104308.

[4] T. Gravestock, M. Blitz, W. Bloss and D. E. Heard, ChemPhysChem, 2010, **11**, 3928.